ACS OMEGA

http://pubs.acs.org/journal/acsodf

Article

A Biocompatible, pH-Sensitive, and Magnetically Separable Superparamagnetic Hydrogel Nanocomposite as an Efficient Platform for the Removal of Cationic Dyes in Wastewater Treatment

Rinki Singh, Vikas Munya, Venkata Narayana Are, Debasis Nayak, and Sudeshna Chattopadhyay*

Cite This: *ACS Omega* 2021, 6, 23139−23154

Read Online

ACCESS | Metrics & More | Article Recommendations | Supporting Information

ABSTRACT: A series of environment-friendly cationic dye adsorbents, namely, pH-sensitive superparamagnetic hydrogel nanocomposite AA-VSA-P/SPIONs systems with different concentrations of superparamagnetic iron oxide nanoparticles (SPIONs; 1.2, 3.2, and 5.2 wt %), was synthesized by free-radical polymerization reaction using two pH-sensitive monomers, acrylic acid (AA) and vinylsulfonic acid (VSA), in an optimum ratio, in the presence of presynthesized SPIONs. The structural properties, thermal stability, and chemical configuration of AA-VSA-P/SPIONs systems with different weight percentages of SPIONs were characterized by XRD, TGA, Raman spectroscopy, and FTIR spectroscopy. The systems show substantial efficiency as dye adsorbents for removing cationic dyes (MB dye) from aqueous solution in neutral to alkaline medium. Further, these systems exhibit easy magnetic separation capabilities from aqueous solutions after dye adsorption, even for a very low weight percentage of SPIONs. The adsorption kinetics, mechanism, and isotherms of these systems were evaluated. The study suggests consistency with the pseudo-second-order kinetic model, following an intraparticle diffusion mechanism, where the heterogeneous surface of the system having different activation energies for adsorption plays the crucial role in dye adsorption via chemisorption for higher pH medium, which was further substantiated by excellent data fit with the Freundlich isotherm model. Biocompatibility and regeneration-ability studies establish the environment-friendliness and cost effectivity of the system.

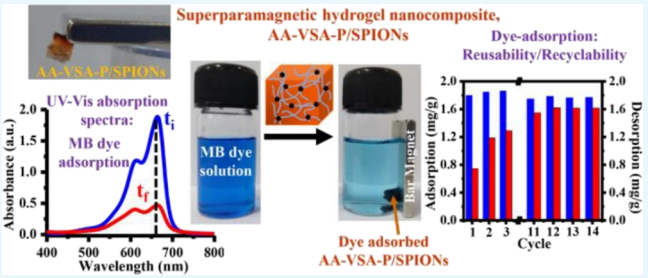

1. INTRODUCTION

Owing to huge industrial application and demand, the production capacity of synthetic dyes has seen drastic augmentation. The current level of synthetic dye production capacity is reported to be as high as more than 700,000 tonnes/year for the purpose of the extensive industrial application.[1] In fact, despite being serious pollutant sources to water resources, synthetic dyes in large numbers are being indiscriminately discharged from various industries, mainly textiles, cosmetics, papering and pulping, leathering, printing, painting, dyeing and dye manufacturing, and so on, bringing about severe environmental problems. The major portion of these synthetic dyes is comprised of cationic dyes, which can do great harm to the environment after getting discharged into water.[2] For example, the cationic methylene blue (MB) dye is widely used and finds application in different industries, especially in the textile and dyeing industries. MB dye is also used in many pharmaceutical applications.[3,4] MB causes eye and skin irritation in case of short-term exposure, whereas exposure for a long time may result in nausea, breathing difficulty, increased heart rate, gastritis, and mental confusion.[4−6] Basically, the dyes in the effluent make it highly alkaline since the processes such as reduction of polyester fabrics and mercerization of cottons employ caustic alkali.[7] Generally, textile industries generate dyeing discharge with pH ranging around 9−11.[8,9] Thus, it is of utmost importance that MB is completely removed from the industrial waste prior to their discharge. Releasing dye-containing wastewater into water bodies and/or ground water poses serious problems in environmental protection and wastewater treatment. Furthermore, the effluent without any treatment decreases water transparency and the oxygen transfer rate into water.[10,11] It even would adversely influence the photosynthesis by plants in the aquatic systems.[12] Moreover, dyes are generally toxic to living creatures and cannot be easily degraded by microorganisms.[13] Therefore, cost-effective techniques for efficiently removing dye contaminants from wastewater are highly desirable. Currently, various technologies are available and applied for the removal of dyes from wastewater, including coagulation/flocculation, photocatalysis, ultrafiltration, biosorption, Fenton-biological treatment, oxidation, and adsorp-

Received: May 25, 2021
Accepted: August 20, 2021
Published: August 31, 2021

tion.[4,14] Among various dye removal strategies, adsorption is considered to be the simplest and best because of its low cost, ease of operation, high efficiency, regeneration, insensitivity to toxic substances, and lack of secondary pollution.[15,16] In addition to the choice of removal strategies, designing a low-cost, eco-friendly, and more efficient adsorbent is another critical aspect of water remediation.[16] Diverse adsorbents have been developed for the adsorption process such as activated carbon (AC), graphene oxide, zeolites, clay, agriculture waste, mGO/PVA CGs, multiwalled carbon nanotube/xylan hydrogel, etc.[15,17] However, with these materials, major difficulty is faced at the time of separation from the solution, although they have good adsorption ability. To compensate for these inadequacies, fabrication of environment-friendly materials with selective adsorption of dyes and easy separation capability has been attempted.[18] The hydrogels especially composed of renewable and sustainable sources have been used for treatment of colored water.[19,20] Hydrogels are three-dimensional cross-linked polymers containing hydrophilic groups, which enable them to absorb water. They have chemically responsive functional groups, which enable them to capture dyes from wastewater and to release these toxic pollutants upon changes in aqueous solution conditions. The hydrophilic nature of hydrogels enables them to possibly form a flexible network of polymer chains, which allow solutes to penetrate into the network with water and form stable complexes with the functional groups.[15,21] Great attention is given to stimuli-responsive hydrogels, as these hydrogels show dramatic changes in volume and properties in response to external stimuli such as temperature, pH, ionic strength, electric field, etc. They can swell and shrink according to the external condition (or surroundings, which makes them attractive for use as intelligent materials (smart gels)).[22,23] Wastewater pH has been found to be one of the parameters that affect the process of wastewater treatment directly. A pH-sensitive hydrogel, having anionic (acidic) groups (e.g., carboxylic acid or sulfonic acid pendant groups) or cationic (basic) groups such as amine pendant group, can either accept or release protons, respectively, in response to pH change, thus being capable of adsorbing ionic dyes and becoming useful for wastewater treatment, where the great influence of pH is evident.[15,24]

Recently, pH-responsive magnetic hydrogels are emerging as a new generation of adsorbents for environmental purification because of the underlying benefits that dye-adsorbed hydrogels are readily separable from dye solution by an external magnetic field.[25,26] Compared with other traditional separation techniques such as filtration and centrifugation, the magnetic separation process is easy to operate with high separation efficiency and low cost.[27] Magnetic separation is one of the promising methods of environmental remediation, because it produces no contaminants such as flocculants and it has the capability of treating large amounts of wastewater within a short time.

Herein, we report the synthesis and characterization of an efficient pH-sensitive, dual-responsive (pH and magnetic field) superparamagnetic hydrogel toward its application as an efficient dye adsorbent for wastewater treatment and its response toward magnetic separation for the environmental remediation or wastewater treatment process. Dual-responsive superparamagnetic hydrogel nanocomposites (AA-VSA-P/SPIONs) were synthesized using free radical polymerization of two pH-sensitive monomers, acrylic acid (AA) and vinylsulfonic acid (VSA), in the presence of presynthesized superparamagnetic iron oxide nanoparticles (SPIONs, Fe_3O_4). The optimization of the concentration of SPIONs (i.e., Fe_3O_4 nanoparticles) in the AA-VSA-P/SPIONs system for its efficacy in dye adsorption application and the consequent response in the magnetic separation process (for dye-adsorbed superparamagnetic hydrogel) have been explored. The thermal stability, structural properties, and chemical configuration of synthesized AA-VSA-P/SPIONs systems with different weight percentages (1.2, 3.2, and 5.2 wt %) of SPIONs were studied and characterized by thermogravimetric analysis (TGA), X-ray diffraction analysis (XRD), Raman spectroscopy, and Fourier transform infrared (FTIR) spectroscopy. Superparamagnetic properties of SPIONs and AA-VSA-P/SPIONs systems were confirmed by measuring the magnetization (M) as a function of the applied magnetic field (H) using a Quantum Design MPMS XL superconducting quantum interference device magnetometer. The pertinence of synthesized superparamagnetic hydrogels, AA-VSA-P/SPIONs with different weight percentages (1.2, 3.2, and 5.2 wt %) of SPIONs, for the MB dye adsorption from the aqueous solution was evaluated based on adsorption capacity, response/sensitivity of the dye-adsorbed hydrogel toward the magnetic field-mediated separation process, and a detailed study on adsorption kinetics, mechanism, and isotherm. Furthermore, recyclability/reusability and biocompatibility/eco-friendliness were examined in view of its practical applicability in the dye adsorption process for wastewater treatment.

2. RESULTS AND DISCUSSION

AA-VSA-P/SPIONs with different concentrations of SPIONs were synthesized from their monomers AA and VSA by free-radical polymerization reaction, in the presence of the initiator BPO and the cross-linker EGDMA, and the addition of presynthesized SPIONs at different weight percentages (1.2, 3.2, and 5.2 wt %) of SPIONs. The three-dimensional network structure was created by the use of a cross-linking agent, which helps hold water and solute molecules into it.[15] Simultaneously, the purpose of inclusion of SPIONs in the hydrogel was to induce the superparamagnetic property in the system. As mentioned above, different weight percentages of SPIONs within the hydrogel systems (AA-VSA-P/SPIONs-I, AA-VSA-P/SPIONs-II, and AA-VSA-P/SPIONs-III) were studied to explore the influence of incorporation of SPIONs into the AA-VSA-P/SPIONs composite hydrogel system on the dye adsorption process (kinetics, mechanism), efficiency, and their sensitivity/response toward the magnetic separation process. The incorporation of SPIONs (i.e., Fe_3O_4 nanoparticles) in the hydrogel matrix offers a magnetic behavior to the hydrogel systems, and subsequently, the systems were observed to be attracted toward the conventional permanent magnet as shown in Figure 1b. The schematic of the formation of AA-VSA-P/SPIONs with different weight percentages (1.2, 3.2, and 5.2 wt %) of SPIONs is shown in Figure 1a,b. It should be noted that synthesis of the AA-VSA-P/SPIONs system with a higher concentration (wt %) of SPIONs (i.e., above ~6 wt %) was also attempted, which ended up with an impairment in the hydrogel formation process (as shown in Figure S1, Supporting Information).

The structural properties of SPIONs and AA-VSA-P/SPIONs composite hydrogels, AA-VSA-P/SPIONs-I, AA-VSA-P/SPIONs-II, and AA-VSA-P/SPIONs-III, were studied using the X-ray diffraction (XRD) technique. The magnetite

https://doi.org/10.1021/acsomega.1c02720
ACS Omega 2021, 6, 23139−23154

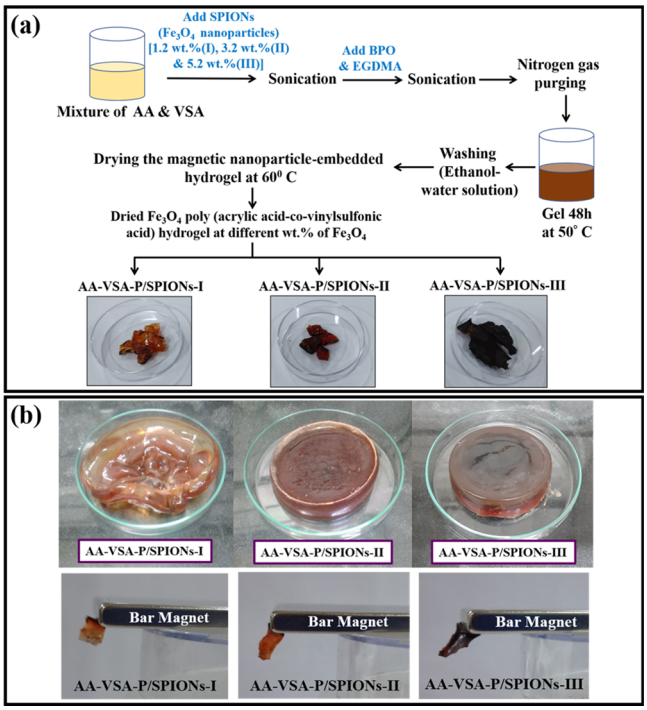

Figure 1. (a) Schematic representation of the synthesis of AA-VSA-P/SPIONs with different concentrations (wt %) of SPIONs, i.e., 1.2 wt % SPIONs (AA-VSA-P/SPIONs-I), 3.2 wt % SPIONs (AA-VSA-P/SPIONs-II), and 5.2 wt % SPIONs (AA-VSA-P/SPIONs-III); (b) photographs showing the formation of AA-VSA-P/SPIONs with different weight percentages of SPIONs and their magnetic attraction toward the conventional permanent bar magnet (180 mT).

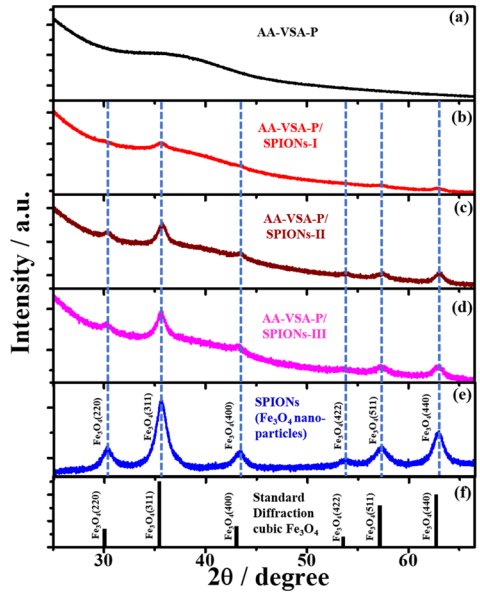

Figure 2. X-ray diffraction patterns of (a) the AA-VSA-P hydrogel, (b) AA-VSA-P/SPIONs-I, (c) AA-VSA-P/SPIONs-II, (d) AA-VSA-P/SPIONs-III, (e) synthesized SPIONs (i.e., Fe_3O_4 nanoparticles), and (f) reference data, the standard diffraction pattern of cubic Fe_3O_4 with a space group of $Fd\bar{3}m$ (227) (JCPDS PDF card no. 00-001-1111).

phase (Fe_3O_4) of synthesized iron oxide nanoparticles in AA-VSA-P/SPIONs-I, AA-VSA-P/SPIONs-II, and AA-VSA-P/SPIONs-III was confirmed by the XRD study.

2.1. X-ray Diffraction Analysis (XRD). The existence and crystallinity of SPIONs (i.e., Fe_3O_4 nanoparticles) in synthesized AA-VSA-P/SPIONs-I, AA-VSA-P/SPIONs-II, and AA-VSA-P/SPIONs-III were investigated by the XRD analysis, as shown in Figure 2, along with XRD data of pristine SPIONs (i.e., Fe_3O_4 nanoparticles) and AA-VSA-P hydrogel. The AA-VSA-P hydrogel shows amorphous nature, which is consistent with the characteristic structural properties of the polymer.[28] Figure 2 demonstrates that the diffraction patterns of synthesized pristine iron oxide nanoparticles (i.e., SPIONs or Fe_3O_4 nanoparticles) and superparamagnetic hydrogel nanocomposites (with different weight percentages of SPIONs) match with the standard diffraction pattern of cubic Fe_3O_4 (magnetite) with a space group of $Fd\bar{3}m$ (227) (JCPDS PDF card no. 00-001-1111). The study reveals that the synthesized iron oxide nanoparticles have a magnetite phase, i.e., a Fe_3O_4 crystal structure.[29] The results also demonstrate the enhancement in characteristic SPIONs (i.e., Fe_3O_4 nanoparticles) diffraction peaks in the synthesized AA-VSA-P/SPIONs with increasing wt % of SPIONs in it, confirming an increase in the SPIONs loading in the hydrogel matrix. It should be noted that XRD patterns of synthesized AA-VSA-P/SPIONs systems only exhibited the standard diffraction peaks corresponding to cubic Fe_3O_4 (magnetite),[29] as displayed in Figure 2. The absence of any additional XRD peaks for AA-VSA-P/SPIONs systems assured that the hybridization process has not given rise to any phase change of the magnetic iron oxide (SPIONs, Fe_3O_4) or there are no extra magnetic phases (such as α-Fe_2O_3 and γ-Fe_2O_3[30,31]) that have been included into the hydrogel nanocomposites during the synthesis process; thus, the synthesized AA-VSA-P/SPIONs-I, AA-VSA-P/SPIONs-II, and AA-VSA-P/SPIONs-III maintain the magnetic properties of SPIONs (i.e., Fe_3O_4 nanoparticles).

Debye−Scherrer expression was utilized to evaluate the average particle size of SPIONs.[28]

$$D = \frac{K\lambda}{\beta \cos\theta} \quad (1)$$

where D, K, and β denote respectively the average size of the crystallites, shape factor (K = 0.94, considering the spherical shape of SPIONs), and full width at half-maximum of the highest intensity diffraction peak at angle θ. λ is the X-ray wavelength. The estimated average size of SPIONs was ∼8 nm as extracted from XRD patterns of pristine SPIONs and different sets of AA-VSA-P/SPIONs composite hydrogels (AA-VSA-P/SPIONs-I, AA-VSA-P/SPIONs-II, and AA-VSA-P/SPIONs-III). Furthermore, the average size of the synthesized Fe_3O_4 nanoparticles was also confirmed by transmission electron microscopy (TEM), as shown in Figure S2, Supporting Information.

A point worth highlighting is that in this study, the superparamagnetic properties of the synthesized SPIONs and characteristic AA-VSA-P/SPIONs composite hydrogel systems, i.e., AA-VSA-P with 1.2 and 3.2 wt % SPIONs, AA-VSA-P/SPIONs-I and AA-VSA-P/SPIONs-II, were explored and confirmed by a Quantum Design MPMS XL superconducting quantum interference device magnetometer at room temperature, as discussed in S3 and Figure S3, Supporting Information, and such observed superparamagnetic behavior is consistent with our previous study.[28]

2.2. Spectroscopic Analysis: Fourier Transform Infrared (FTIR) and Raman Spectroscopy. FTIR and Raman

https://doi.org/10.1021/acsomega.1c02720
ACS Omega 2021, 6, 23139−23154

spectroscopy techniques were utilized to evaluate the chemical configuration of the AA-VSA-P/SPIONs composite hydrogel systems (i.e., AA-VSA-P/SPIONs-I, AA-VSA-P/SPIONs-II, and AA-VSA-P/SPIONs-III).

2.2.1. FTIR Spectroscopy. ATR-FTIR spectra of SPIONs (i.e., Fe_3O_4 nanoparticles), the pristine hydrogel AA-VSA-P, and superparamagnetic nanocomposite hydrogels, AA-VSA-P/SPIONs-I, AA-VSA-P/SPIONs-II, and AA-VSA-P/SPIONs-III, are illustrated in Figure 3. The presence of characteristic

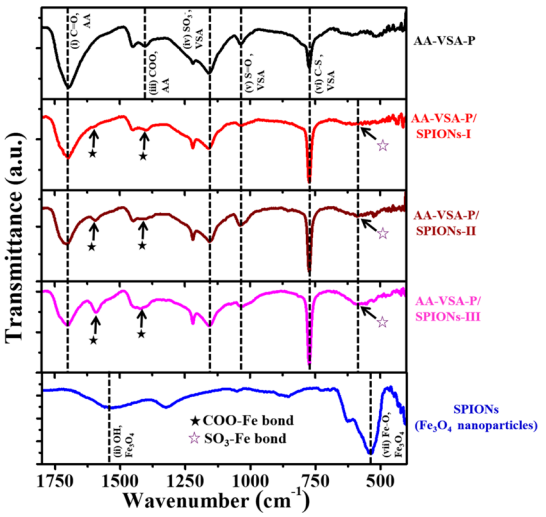

Figure 3. ATR-FTIR spectra of SPIONs (Fe_3O_4 nanoparticles), AA-VSA-P hydrogel, and AA-VSA-P/SPIONs/PAAVSA-I, AA-VSA-P/SPIONs-II, and AA-VSA-P/SPIONs-III hydrogels. For AA-VSA-P/SPIONs systems, an additional band at 1589 cm^{-1} is attributed to the COO−Fe bond, the ATR-FTIR band at 1407 cm^{-1} with lower relative intensity and a slight peak shift is assigned to the interaction of SPIONs and carboxylate ions (COO^-) (represented by solid stars), and the band at 576 cm^{-1} is assigned to the interaction of the SO_3^- group with the SPIONs (i.e., Fe_3O_4 nanoparticles) (represented by open stars).

bands of AA and VSA in the ATR-FTIR spectrum of the superparamagnetic nanocomposite hydrogels is shown in Figure 3. The spectra of pristine (AA-VSA-P) and composite (AA-VSA-P/SPIONs) hydrogels show the bands at 1714 and 1407 cm^{-1} corresponding to the stretching vibration of (—C═O) and symmetric stretching vibration of COO^- of acrylic acid (AA), respectively.[32] The bands at 1170, 1040, and 774 cm^{-1} are ascribed to the $-SO_3^-$ symmetric stretching vibration,[15] S═O stretching vibration, and C−S antisymmetric stretching modes of vinylsulfonic acid (VSA), respectively.[15,33] Also, the spectra of pristine SPIONs (Fe_3O_4 nanoparticles) show the characteristic bands at 1530 and 540 cm^{-1} representing the −OH bending vibration mode[34] and Fe−O stretching vibration mode, respectively.[35] Furthermore, the absorption band at 1407 cm^{-1} in the ATR-FTIR spectrum of AA-VSA-P/SPIONs composite hydrogels shows a change in relative intensity and a slight peak shift, implying the interaction of SPIONs and carboxylate ions (COO^-) of the hydrogels. Also, the ATR-FTIR spectra of AA-VSA-P/SPIONs composite hydrogels indicate an additional absorption band at 1589 cm^{-1}, which is consistent with the characteristic band of the COO−Fe bond, while concomitant to the increasing concentration of SPIONs (i.e., Fe_3O_4 nanoparticles), the intensity of the said peak increases.[36,37] In addition, the emergence of a peak at about 576 cm^{-1} in the spectra of AA-VSA-P/SPIONs magnetic hydrogels, with enhanced intensity with increasing concentration of SPIONs (i.e., Fe_3O_4 nanoparticles) in it, indicates an interaction of SPIONs, with the SO_3^- functional group[38] in AA-VSA-P/SPIONs systems, signifying further the association of SPIONs with the AA-VSA-P chain.

2.2.2. Raman Spectroscopy. Raman spectra of AA-VSA-P/SPIONs for a characteristic sample (with 5.2 wt % SPIONs in AA-VSA-P, i.e., AA-VSA-P/SPIONs-III) are displayed in Figure 4. The reference spectra of the AA-VSA-P hydrogel

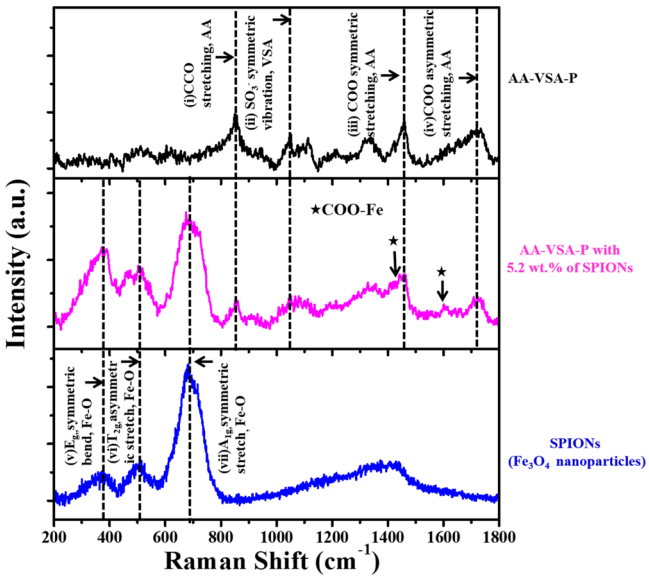

Figure 4. Raman spectra of the pristine hydrogel AA-VSA-P, composite hydrogel AA-VSA-P/SPIONs-III (i.e., AA-VSA-P with 5.2 wt % SPIONs), and SPIONs. For the AA-VSA-P/SPIONs composite hydrogel, the additional peaks at 1431 and 1597 cm^{-1} (COO^- and Fe complex) are represented by solid stars.

and SPIONs are also illustrated in Figure 4. The Raman data have been collected using a 633 nm laser for these sets of samples. Characteristic peaks of the magnetite phase at 350 cm^{-1} (E_g), 500 cm^{-1} (T_{2g}), and 700 cm^{-1} (A_{1g})[28] were evident in the spectra of AA-VSA-P/SPIONs composite hydrogels and pristine SPIONs. The results confirm the formation of the Fe_3O_4 (i.e., magnetite) phase of SPIONs, which is consistent with the XRD results. The Raman peaks corresponding to the pristine hydrogel AA-VSA-P at 855, 1456, and 1707 cm^{-1} in correlation with the CCO stretching, COO symmetric stretching, and COO asymmetric stretching of acrylic acid (AA) and the band at 1043 cm^{-1}, ascribed to the $-SO_3^-$ symmetric vibrational mode of vinylsulfonic acid (VSA),[15] are also evident in the composite hydrogel (AA-VSA-P/SPIONs-III), as shown in Figure 4. The emergence of additional peaks at 1431 and 1597 cm^{-1} in the Raman spectra of the composite hydrogel AA-VSA-P/SPIONs-III signifies the formation of the COO^- and Fe complex.[28] The results indicate the adherence (binding) of SPIONs with the polymer (AA-VSA-P) chain in the hydrogel network. Such indication of the interaction of SPIONs with the polymer chain in the hydrogel network was also evident in our previous study.[28]

Spectroscopic analyses (FTIR and Raman) imply that the SPIONs (i.e., Fe_3O_4 nanoparticles) interdiffused and disseminated in the polymer matrix during polymerization. The

https://doi.org/10.1021/acsomega.1c02720
ACS Omega 2021, 6, 23139−23154

hydroxide radicals' groups on the surface of SPIONs (i.e., $Fe_3O_4(OH)_x$) interact with COO^- and SO_3^- of AA-VSA-P, which may lead to an efficient embedding of SPIONs into the pristine polymer matrix, resulting in the gradual formation of the AA-VSA-P/SPIONs hydrogel network structure. The observation is consistent for the different weight percentages of SPIONs in the AA-VSA-P system. Additionally, as discussed above, the ATR-FTIR spectra of AA-VSA-P/SPIONs-I, AA-VSA-P/SPIONs-II, and AA-VSA-P/SPIONs-III indicate the emergence of a characteristic COO−Fe band at 1597 cm^{-1} with enhanced intensity with increasing concentration of SPIONs (i.e., Fe_3O_4 nanoparticles) in AA-VSA-P/SPIONs systems, specifying the further interaction process, which is also supported by the Raman results.

2.3. Thermogravimetric Analysis (TGA). Thermogravimetric analysis (TGA) was conducted for the AA-VSA-P/SPIONs superparamagnetic hydrogels for two different concentrations of SPIONs (3.2 and 5.2 wt %) to study the thermal stability of the synthesized superparamagnetic hydrogel nanocomposites with increasing concentration of SPIONs. TGA for pristine AA-VSA-P and SPIONs was also carried out for the reference study, as shown in Figure 5. The results

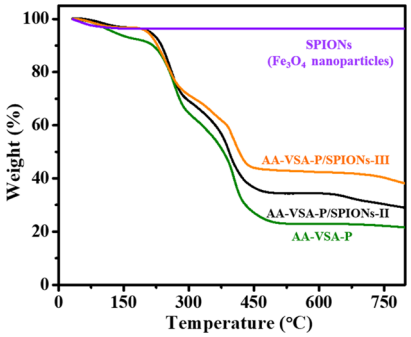

Figure 5. TGA analysis of SPIONs (i.e., Fe_3O_4 magnetic nanoparticles) and AA-VSA-P with 5.2 wt % SPIONs, 3.2 wt % SPIONs, and 0% SPIONs (i.e., AA-VSA-P/SPIONs-III, AA-VSA-P/SPIONs-II, and the AA-VSA-P hydrogel, respectively).

demonstrated that the thermal stability of the superparamagnetic AA-VSA-P/SPIONs hydrogel gets better with increasing concentration of SPIONs in it. Figure 5 reveals that the overall stability of AA-VSA-P/SPIONs composite hydrogel systems is reasonably good (and better than pristine AA-VSA-P) up to 200 °C (where the weight loss is within the range of 2−4%), with the weight reaching about 70% of its original value at about 300 °C. A sharp thermal degradation at about 450 °C is also evident for AA-VSA-P/SPIONs composite systems, similar to pristine AA-VSA-P, as discussed in our previous study.[28] It should be noted that the respective residual weights of AA-VSA-P/SPIONs systems (in the range of 450−800 °C) are also higher in comparison to that of AA-VSA-P, which signifies the effect of incorporation of SPIONs into the system, while the thermal stability exhibits noticeable enhancement with increasing SPIONs concentration into the system. The observed improvement in the thermal stability of AA-VSA-P/SPIONs can be attributed to the effects of the following phenomena:[28] (i) incorporation of SPIONs into the polymer matrix (AA-VSA-P), which can improve its thermal stability, as SPIONs have significantly high thermal stability, as illustrated in Figure 5, and (ii) the effect of SPIONs−polymer matrix interaction that restricts the movement of the polymer's molecular chain and protects the AA-VSA-P matrix from further degradation.[39]

2.4. Dye Adsorption Properties. *2.4.1. Impact of pH Medium.* The pH of the medium plays a vital role on the dye adsorption performance of the hydrogels,[40] as the binding sites of the hydrogels/composites and the ionization process are used to be greatly affected by the pH of the medium.[15] The effect of pH on the dye adsorption performance of superparamagnetic hydrogel composites, AA-VSA-P/SPIONs systems, was explored by using methylene blue dye (MB) solution, one of the common hazardous (toxic) dyes. The pH of the solution shows a critical impact on the methylene blue (MB) dye adsorption process by AA-VSA-P/SPIONs systems, as it altered the degree of protonation of the functional groups and therefore surface charge of the superparamagnetic hydrogel nanocomposites. It should be also noted that, generally, dye-containing wastewater is alkaline (i.e., with high pH values) in nature, as discussed in our earlier study[15] in detail. In this context, the effects of incorporation of different concentrations of SPIONs in AA-VSA-P/SPIONs systems to their dye adsorption performance at different pH values were studied elaborately in this section. The dye adsorption capacity, kinetics, and mechanism for these systems along with their response to the magnetic separation process have been explored and discussed. The dye adsorption properties of AA-VSA-P/SPIONs with different weight percentages of SPIONs, i.e., 1.2 wt % (i.e., AA-VSA-P/SPIONs-I), 3.2 wt % (i.e., AA-VSA-P/SPIONs-II), and 5.2 wt.% (i.e., AA-VSA-P/SPIONs-III), were demonstrated by using MB dye solution at different characteristic pH values, such as pH 9, 7, and 1.4, as displayed in Figure 6a−c. All these measurements were conducted at room temperature.

Approximately 0.3 g of AA-VSA-P/SPIONs-I, AA-VSA-P/SPIONs-II, and AA-VSA-P/SPIONs-III magnetic hydrogels was immersed separately in three sets of 0.05 L solution of methylene blue dye (12 mg/L), respectively. Figure 6b,c shows the UV−Vis absorption spectra of the MB dye solution that were collected at different time intervals to evaluate the variation in the content of methylene blue dye (MB) in the solution due to the adsorption by the superparamagnetic hydrogels. Here, the changes in the normalized concentration (C/C_0) of MB with time due to adsorption by superparamagnetic hydrogel nanocomposites, AA-VSA-P/SPIONs systems, with different SPIONs contents, are considered to be proportional to the respective normalized MB dye absorbance (A/A_0) at the main peak (at the wavelength of 664 nm) of the absorption spectrum of the MB dye solution (Figure 6c).[15] For a given pH value, C_0 and C_t are the initial concentration and instantaneous MB dye concentration (in the dye solution) after adsorption by superparamagnetic hydrogel nanocomposites, respectively.

The instantaneous dye adsorption capacity q_t (mg/g) was estimated by eq 2, where the weight of adsorbed dye and superparamagnetic hydrogel adsorbents are represented in mg and g, respectively:[12,15]

$$q_t = \frac{(C_0 - C_t)V}{W} \quad (2)$$

where C_0 (mg/L) and C_t (mg/L), respectively, are the initial and instantaneous dye concentrations in the solution after adsorption by magnetic hydrogels. V (in L) represents the volume of the MB dye solution, and W (in g) represents the primary weight of the dry magnetic hydrogel before swelling.

https://doi.org/10.1021/acsomega.1c02720
ACS Omega 2021, 6, 23139−23154

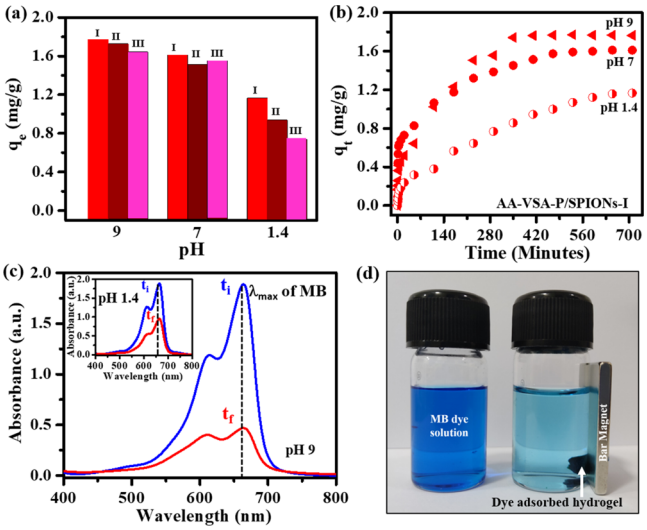

Figure 6. (a) Equilibrium adsorption capacity (q_e) of superparamagnetic hydrogel nanocomposites with different wt % of SPIONs: AA-VSA-P/SPIONs-I, AA-VSA-P/SPIONs-II, and AA-VSA-P/SPIONs-III; (b) adsorption behavior: effect of contact time on the MB dye uptake by AA-VSA-P/SPIONs-I (initial MB concentration is 12 mg/L, at pH 9, pH 7, and pH 1.4); (c) UV–Vis absorbance spectra of MB dye solution at the initial stage (t_i), i.e., before the adsorption, and at the equilibrium stage after adsorption (t_f) by the AA-VSA-P/SPIONs-I hydrogel at pH 9 and pH 1.4; (d) photograph of dye adsorption and subsequent magnetic separation phenomena before and after dye adsorption by AA-VSA-P/SPIONs-I at pH 9 and the dye-adsorbed hydrogel magnetically separated by a bar magnet (180 mT).

The impact of pH values of the medium on MB dye removal by the superparamagnetic nanocomposite hydrogels, AA-VSA-P/SPIONs-I, AA-VSA-P/SPIONs-II, and AA-VSA-P/SPIONs-III, was examined under pre-optimized time for a given set of fixed parameters (C_0, V, and W). The results demonstrate the vital role of pH of the medium in this context, which are displayed in Figure 6.

The dye adsorption capacities of AA-VSA-P/SPIONs-I, AA-VSA-P/SPIONs-II, and AA-VSA-P/SPIONs-III at different pH values, in the equilibrium stage, are shown in Figure 6a. The dye adsorption behavior (adsorption capacity as a function of time) of a characteristic AA-VSA-P/SPIONs system (AA-VSA-P/SPIONs-I) at different pH values is displayed in Figure 6b. The results reveal that the maximum adsorption (or equilibrium adsorption) of MB dye increases significantly with increasing pH value from 1.4 to 9, while such a trend is consistent with the observation discussed in our previous study[15] for the dye adsorption behavior of pristine hydrogel (i.e., AA-VSA-P). The observed high dye adsorption capacity of AA-VSA-P/SPIONs composite hydrogels at higher pH values (e.g., pH 7 and pH 9) makes them significant for dye removal in wastewater treatment (where the dye-containing wastewater generally has high pH, as discussed earlier). The observation on the dye adsorption capacities of the AA-VSA-P/SPIONs-I, AA-VSA-P/SPIONs-II, and AA-VSA-P/SPIONs-III, which increase with increasing pH value, can be ascribed to the ionization of the carboxylic groups and sulfonic groups of AA and VSA, respectively. At a higher pH value, the carboxylic groups and sulfonic groups of AA-VSA-P and hydroxyl groups of $Fe_3O_4(OH)_x$ become ionized, which would increase the electrostatic attraction between negatively charged functional groups (COO^- and SO_3^-) of AA, VSA, and positively charged cationic MB dye and possible hydrogen bonding between $Fe_3O_4(OH)_x$ and MB dye.[15,25] Also, at a higher pH value, the ionized groups present on the superparamagnetic hydrogel nanocomposites develop the electrostatic repulsive interactions among the adjacent ionized groups, causing an expansion in the polymer network and resulting in an increase in the MB dye absorption.[15] In contrast, at a lower pH value, the decrease in adsorption occurs due to the competition among excess hydrogen ions and MB molecules (a cationic dye) to occupy the adsorption sites.[15]

Furthermore, the results reveal that the equilibrium adsorption capacity (q_e) of AA-VSA-P/SPIONs decreases with the increase in SPIONs content, as displayed in Figure 6a. AA-VSA-P with 1.2 wt % SPIONs content (i.e., AA-VSA-P/SPIONs-I) shows maximum dye adsorption capacity with respect to the magnetic hydrogels with higher wt % of SPIONs (i.e., AA-VSA-P/SPIONs-II and AA-VSA-P/SPIONs-III). The results can be ascribed to the fact that in the presence of a higher number of SPIONs (i.e., Fe_3O_4 nanoparticles), more SPIONs acted as an additional network point (through the interaction of SPIONs, i.e., Fe_3O_4 nanoparticles, $Fe_3O_4(OH)_x$ with COO^- and SO_3^- groups, as discussed in Section 2.2), and accordingly, the cross-link density of the magnetic hydrogel became larger, which also leads to the lowering of the available number of COO^- and SO_3^- groups to interact with MB dye (as discussed earlier to explain the dye adsorption mechanism by the AA-VSA-P hydrogel), which may cause the observed drop in the equilibrium adsorption capacity of MB dye[1,41] for the AA-VSA-P/SPIONs hydrogel with higher Fe_3O_4 content (Figure 6a). In view of the observed higher dye adsorption capacity of AA-VSA-P/SPIONs-I in comparison to AA-VSA-P with a higher concentration of SPIONs, AA-VSA-P/SPIONs-II, and AA-VSA-P/SPIONs-III, it was essential to investigate the potential of dye-adsorbed AA-VSA-P with the lowest concentration of SPIONs, i.e., dye-adsorbed AA-VSA-P/SPIONs-I, to respond toward the magnetic separation process. In this context, it should be further noted that the objective in this case was to achieve the superparamagnetic properties in the dye-adsorbing hydrogel by incorporating SPIONs into it to give it the capabilities to be separated out through the magnetic separation process. Figure 6d shows the dye adsorption and subsequent magnetic separation phenomena for AA-VSA-P/SPIONs-I at pH 9. The figure displays the MB dye solution at alkaline/high pH (pH 9) before and after dye adsorption by AA-VSA-P/SPIONs-I and the excellent capabilities of dye-adsorbed AA-VSA-P/SPIONs-I to be magnetically separated out by a bar magnet of nominal strength (180 mT), indicating the potential of the AA-VSA-P/SPIONs system for the dye-contaminated wastewater treatment.

In view of the above discussion, the detailed kinetics/mechanism of the dye adsorption process via AA-VSA-P/SPIONs, the superparamagnetic composite hydrogels, was studied for better understanding of the system and the process, which is crucial for further applications and possible future improvement. The studies on dye adsorption kinetics and mechanism have been discussed in the following sections.

2.5. Dye Adsorption Kinetics. The study of kinetic behavior is an essential path to explain the adsorption interactions. The dye adsorption kinetics of AA-VSA-P/SPIONs with different weight percentages (1.2, 3.2, and 5.2

https://doi.org/10.1021/acsomega.1c02720
ACS Omega 2021, 6, 23139−23154

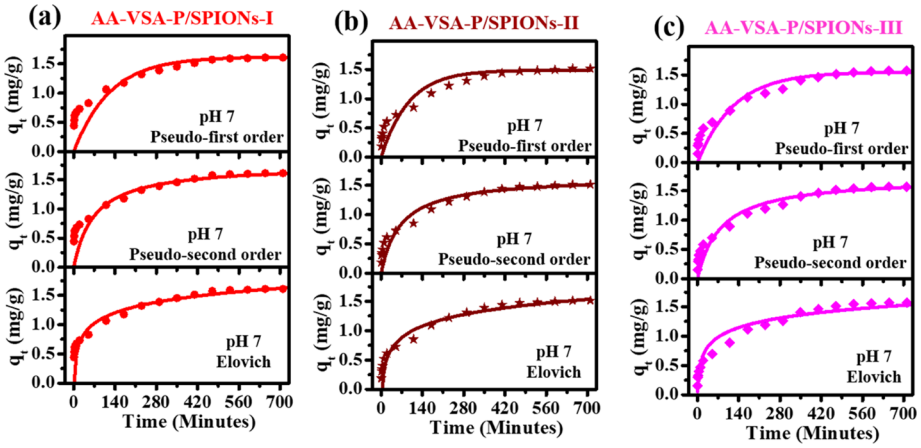

Figure 7. MB dye adsorption at pH 7 by (a) AA-VSA-P/SPIONs-I, (b) AA-VSA-P/SPIONs-II, and (c) AA-VSA-P/SPIONs-III: experimental data fit with various kinetic models, pseudo-first-order (top panel), pseudo-second-order (middle panel), and Elovich equations (bottom panel).

wt %) of SPIONs were explored by fitting the experimental data for q_t vs time (t) using various kinetic models including pseudo-first-order (PFO), pseudo-second-order (PSO), and Elovich models.[15,16,42]

2.5.1. Pseudo-first-order and Pseudo-second-order Models. The pseudo-first-order kinetic model explains the physical adsorption of adsorbate by the adsorbent,[43] is applicable for the adsorption process in solid−liquid systems, as proposed by Lagergren,[44] and is expressed by the following equation:[15]

$$\frac{dq_t}{dt} = k_1(q_e - q_t) \tag{3}$$

where q_e and q_t represent the adsorption capacity at equilibrium and at instantaneous time t, respectively (where the weights of adsorbed dye and magnetic hydrogel adsorbent are in mg and g, respectively, and subsequently, the adsorption capacity is in mg/g).[15] k_1 (min^{-1}) represents the adsorption rate constant.

Upon integrating using the initial conditions of $q_t = 0$ when $t = 0$,[45] eq 3 yields:

$$q_t = q_e(1 - e^{-k_1 t}) \tag{4}$$

The pseudo-second-order kinetic model describes the process predicting the adsorption of dye by the surface of the adsorbent through chemisorption,[16,46] as suggested by Ho and Mckay,[47] and is expressed as follows:[15,16]

$$\frac{dq_t}{dt} = k_2(q_e - q_t)^2 \tag{5}$$

Integrating eq 5 with the boundary conditions results in:

$$q_t = \frac{q_e^2 k_2 t}{1 + q_e k_2 t} \tag{6}$$

where q_e, q_t, and t are already defined above. k_2 (g mg^{-1} min^{-1}) represents the overall adsorption rate constant for this model.

2.5.2. Elovich Kinetic Model. The Elovich model has been extensively utilized in adsorption kinetics to define the chemical adsorption process where the adsorbing surface is heterogeneous and the surface has different activation energies for the adsorption of dye.[15,48] Many chemisorption adsorption processes have been described appropriately using this model.[49]

The equations related to this model are as follows:

$$\frac{dq_t}{dt} = \alpha e^{-\beta q_t} \tag{7}$$

Integration using the boundary conditions yields:

$$q_t = \frac{1}{\beta}\ln(\alpha\beta t) \tag{8}$$

$$q_t = \left(\frac{1}{\beta}\right)\ln(\alpha\beta) + \left(\frac{1}{\beta}\right)\ln(t) \tag{9}$$

where α (mg g^{-1} min^{-1}) represents the initial adsorption rate of adsorbate by the adsorbent; β (g mg^{-1}) is associated with the extent of surface coverage and activation energy for chemisorption.[48]

The dye adsorption behavior of AA-VSA-P/SPIONs-I, AA-VSA-P/SPIONs-II, and AA-VSA-P/SPIONs-III at a higher pH value (pH 7) was analyzed, and it is shown in Figure 7. Figure 7 displays the plot from fits that were obtained by fitting the experimental data with pseudo-first-order, pseudo-second order, and Elovich kinetic models using eqs 4, 6, and 9, as mentioned above. The best fit parameters for the three kinetic models are shown in Table 1. The correlation coefficient (R^2), as summarized in Table 1 (along with the best fit parameters), offers a quantitative estimation of the pertinence of the best adsorption kinetic model to explain the experimental data.[15,40] The results reveal that the adsorption of MB dye by AA-VSA-P/SPIONs composite hydrogel systems at a higher pH value with respect to time was better fitted by the pseudo-second-order equation over the pseudo-first-order equation, as shown in the top and middle panels of Figure 7a−c, indicating that the adsorption process on the whole was predominantly controlled by chemisorption.[25,50] In addition, the good quality of fit by the Elovich model, as shown in bottom panels of Figure 7a−c, provides further insights into the kinetics, indicating the chemisorption process through the heterogeneous adsorbing surface, having different activation energies for dye adsorption.[49,51]

In summary, results reveal that the MB dye adsorption by superparamagnetic nanocomposite hydrogels AA-VSA-P/SPIONs is predominantly governed by the chemisorption process where the contribution of the heterogeneous surface of the adsorbant is evident.

https://doi.org/10.1021/acsomega.1c02720
ACS Omega 2021, 6, 23139−23154

Table 1. Summary of Results for Experimental Data Fitting by Different Kinetic Models for the MB Dye Adsorption by AA-VSA-P/SPIONs-I, AA-VSA-P/SPIONs-II, and AA-VSA-P/SPIONs-III at pH 7

			MB (12 mg/L)		
			AA-VSA-P/SPIONs		
pH	kinetic model	parameter	I	II	III
7	pseudo-first-order	k_1 (min^{-1})	0.008	0.01	0.008
		q_e (cal.) (mg/g)	1.62	1.5	1.55
		q_e (exp.) (mg/g)	1.61	1.513	1.57
		R^2	0.46	0.83	0.86
	pseudo-second-order	k_2 (g mg^{-1} min^{-1})	0.008	0.009	0.007
		q_e (cal.) (mg/g)	1.76	1.65	1.74
		q_e (exp.) (mg/g)	1.61	1.513	1.57
		R^2	0.6	0.88	0.9
	Elovich	α (mg g^{-1} min^{-1})	0.19	0.09	0.08
		β (g mg^{-1})	3.85	3.5	3.45
		R^2	0.76	0.81	0.9

The dye adsorption patterns for AA-VSA-P/SPIONs-I and AA-VSA-P/SPIONs-III at low pH (pH 1.4) are also demonstrated in Figure 8. The best fit parameters for the

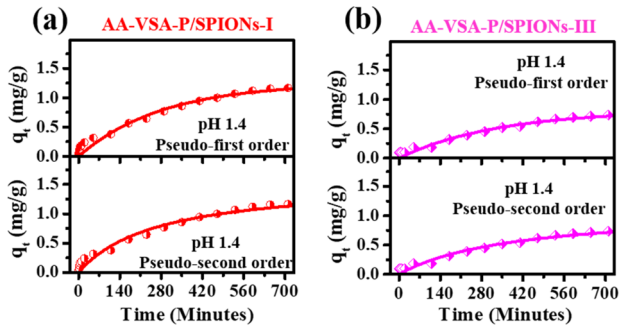

Figure 8. MB dye adsorption at pH 1.4 by (a) AA-VSA-P/SPIONs-I and (b) AA-VSA-P/SPIONs-III: experimental data fit with various kinetic models, pseudo-first-order and pseudo-second-order.

respective kinetic models, along with the correlation coefficient (R^2), are summarized in Table 2. The results demonstrate that at a low pH value, the physical adsorption process plays a significant role along with the chemisorption process in dye adsorption kinetics, exhibiting equally good agreement of the

Table 2. Summary of Results for Experimental Data Fitting by Different Kinetic Models for the MB Dye Adsorption by AA-VSA-P/SPIONs-I and AA-VSA-P/SPIONs-III at pH 1.4

			MB (12 mg/L)	
			AA-VSA-P/SPIONs	
pH	kinetic model	parameter	I	III
1.4	pseudo-first-order	k_1 (min^{-1})	0.004	0.003
		q_e (cal.) (mg/g)	1.25	0.81
		q_e (exp.) (mg/g)	1.16	0.74
		R^2	0.97	0.96
	pseudo-second-order	k_2 (g mg^{-1} min^{-1})	0.002	0.002
		q_e (cal.) (mg/g)	1.56	1.11
		q_e (exp.) (mg/g)	1.16	0.74
		R^2	0.97	0.96

experimental data with the pseudo-first-order model[4,52] and pseudo-second-order model. The results imply that at low pH, the dye adsorption process is mostly limited in the initial stage of adsorption, where the physical adsorption process shows reasonable contribution in determining the overall process and consequent consistency with the pseudo-first-order kinetic model.[52]

It should be noted that while there is a minor effect on equilibrium adsorption capacity (q_e), the overall adsorption rate or rate constant for MB dye adsorption becomes significantly lower in the case of AA-VSA-P/SPIONs, the superparamagnetic composite hydrogels, in comparison to the pristine AA-VSA-P hydrogels at respective pH values. The dye adsorption phenomena for pristine AA-VSA-P have been demonstrated in our previous study.[15] The results can be ascribed to the emergence of an additional network point in the hydrogel due to the incorporation of SPIONs (i.e., Fe_3O_4 nanoparticles, $Fe_3O_4(OH_x)$) through interaction with COO^- and SO_3^- groups, as discussed in Section 2.2), which causes a larger cross-link density and the lowering of reaction sites onto the surface of the hydrogel and essentially reduces the adsorption rate/rate consant of the MB dye adsorption process.

Furthermore, since the adsorption mechanisms play a vital role in determining the factors affecting the adsorption process, the studies on the adsorption mechanism of methylene blue dye by AA-VSA-P/SPIONs-I, AA-VSA-P/SPIONs-II, and AA-VSA-P/SPIONs-III were conducted. In the dye adsorption process, the entire process of solute adsorption onto the composite hydrogel surface may be governed by one or more steps: boundary layer (film) or external diffusion, pore diffusion, surface diffusion, and adsorption onto the pore surface or in a combination of several steps.[53]

From the analysis of the dye adsorption mechanism, as displayed in Figure 9, it was observed that the experimental data can reasonably be described by the intraparticle diffusion model, as given by Weber and Morris.[15]

According to this theory, the adsorbate uptake q_t varies proportionally with the contact's time square root $t^{0.5}$ rather than t.

$$q_t = k_d t^{0.5} + C \tag{10}$$

where k_d (in mg/g $min^{-0.5}$) represents the rate constant for the intraparticle diffusion process. The value of C (mg/g) offers a good assessment about the boundary layer thickness, i.e., the boundary layer effect is larger at a higher value of C.[15]

The q_t vs $t^{0.5}$ plots at three different pH values (pH 7, pH 9, and pH 1.4) are displayed in Figure 9. The results signify that the process of dye adsorption took place in three stages,[15,54] while the fitted data (with eq 10 as mentioned above) and relevant fit parameters are displayed in Figure 9 and Table 3, respectively. The fit parameters (k_d and C_d) are already defined above.[15,55] Among the different stages of the adsorption process, the first stage correlates with the surface adsorption process, which is possibly caused by the driving force due to the high concentration of methylene blue at the initial stage. The second linear segment in the plot represents the second stage of adsorption, which signifies the characteristic of the rate of adsorption in the region, considered as the rate-controlling step through intraparticle diffusion, and is defined by the rate parameter k_{2d}. This gradual adsorption stage assists in the diffusion of MB dye into the superparamagnetic nano-

https://doi.org/10.1021/acsomega.1c02720
ACS Omega 2021, 6, 23139−23154

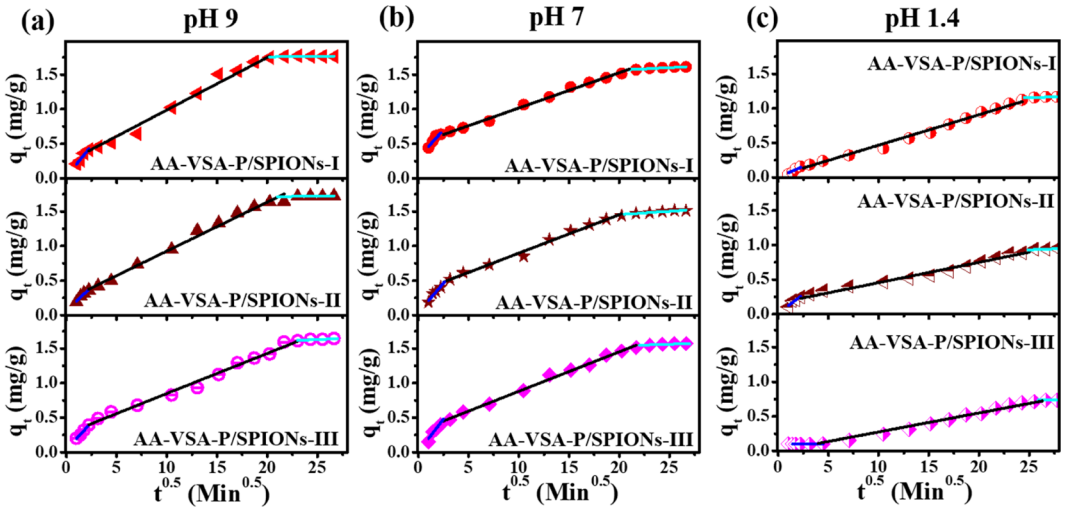

Figure 9. MB dye adsorption by AA-VSA-P/SPIONs-I, AA-VSA-P/SPIONs-II, and AA-VSA-P/SPIONs-III at different pH values, (a) pH 9, (b) pH 7, and (c) pH 1.4: experimental data fit with the intraparticle diffusion model.

Table 3. Summary of Results for Experimental Data Fitting by the Intraparticle Diffusion Model to Explore the MB Dye Adsorption Mechanism onto the Superparamagnetic Nanocomposite Hydrogels at Different pH Media

	AA-VSA-P/SPIONs-I			AA-VSA-P/SPIONs-II			AA-VSA-P/SPIONs-III		
parameter	pH 9	pH 7	pH 1.4	pH 9	pH 7	pH 1.4	pH 9	pH 7	pH 1.4
k_{1d} (mg/g min$^{-0.5}$)	0.18	0.16	0.064	0.14	0.17	0.11	0.16	0.19	0
C_{1d} (mg g^{-1})	0.03	0.3	0.002	0.07	0.04	0.01	0.04	0.008	0.09
R^2	0.93	0.85	0.76	0.93	0.9	0.85	0.99	0.83	1
k_{2d} (mg/g min$^{-0.5}$)	0.08	0.05	0.04	0.07	0.06	0.03	0.06	0.06	0.03
C_{2d} (mg g^{-1})	0.23	0.51	0.03	0.22	0.34	0.18	0.27	0.31	0
R^2	0.98	0.99	0.99	0.99	0.97	0.98	0.99	0.99	0.97
k_{3d} (mg/g min$^{-0.5}$)	0.004	0.008	0	0.003	0.009	0	0.005	0.005	0
C_{3d} (mg g^{-1})	1.67	1.41	1.16	1.65	1.27	0.93	1.5	1.44	0.74
R^2	0.6	0.9	1	0.85	0.93	1	0.77	0.7	1

composite hydrogels. In addition, C_{2d} offers evidence about the boundary layer thickness, which corresponds to the boundary layer diffusion effect.[15,54] Thus, this stage is known as a crucial step. Table 3 exhibits distinctively higher k_d for superparamagnetic nanocomposite hydrogels, AA-VSA-P/SPIONs-I, AA-VSA-P/SPIONs-II, and AA-VSA-P/SPIONs-III, at pH 9 in comparison to acidic pH, implying the greater efficiency in intraparticle diffusion for the superparamagnetic nanocomposite hydrogels at higher pH values (pH 9 and pH 7). The third segment of the plot represents the final equilibrium stage. In this stage, the methylene blue concentration of the remaining solution became low, and subsequently, the diffusion rate slowed down, which finally established the equilibrium condition.

The values of k_d and C_d at different stages of the dye adsorption process by AA-VSA-P/SPIONs composite hydrogel systems at various pH media (pH 9, pH 7, and pH 1.4) were found to follow the relation as $k_{1d} > k_{2d} > k_{3d}$ and $C_{1d} < C_{2d} < C_{3d}$, which can be ascribed to the gradual decrease in MB dye concentration in aqueous solution.[56] Moreover, the results show substantial lower values of C_{1d} and C_{2d} for AA-VSA-P/SPIONs composite hydrogel systems with respect to that of pristine AA-VSA-P (demonstrated in our previous study[15]), indicating that in comparison to pristine AA-VSA-P, the boundary layer effect is much weaker in the first two stages for AA-VSA-P/SPIONs systems, which is consistent with the observed lower adsorption rate (or rate constant) for dye adsorption of AA-VSA-P/SPIONs, as obtained from the kinetic study (Figures 7 and 8 and Tables 1 and 2) and explained elaborately in the earlier sections.

2.6. Dye Adsorption Isotherm. To further investigate the phenomena that occurred on the surface of superparamagnetic hydrogel nanocomposites AA-VSA-P/SPIONs during the adsorption process,[57] the conventional adsorption isotherm models were examined for MB dye adsorption on AA-VSA-P/SPIONs-I, AA-VSA-P/SPIONs-II, and AA-VSA-P/SPIONs-III magnetic hydrogels by conducting multiple separate measurements using different increasing initial concentrations of MB dye solutions. The interaction mechanism of the adsorbent with the adsorbate can be described appropriately through the adsorption isotherm study.[27] Among various isotherm models available in the literature,[15,58,59] Langmuir, Freundlich, and Temkin models are the most broadly used ones to explain the adsorption isotherm.[4,15] The Langmuir isotherm model assumes that the adsorption takes place on a homogeneous adsorbent surface consisting of sites with equal energy and that are equally potent for adsorption. This model is applicable for the continuous monolayer of adsorption, on which no migration of absorbate molecules across the adsorbent surface is expected. The Freundlich adsorption isotherm model considers a heterogeneous adsorption surface, which has uneven accessible sites with diverse adsorption energies. The Temkin adsorption isotherm model offers some further insights into the adsorption process of the heterogeneous

https://doi.org/10.1021/acsomega.1c02720
ACS Omega 2021, 6, 23139−23154

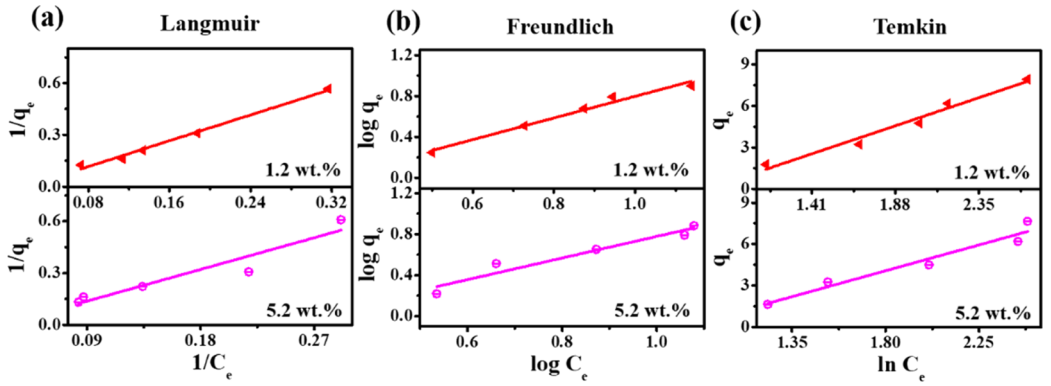

Figure 10. (a) Langmuir, (b) Freundlich, and (c) Temkin isotherm models for MB dye adsorption onto the superparamagnetic hydrogel nanocomposites AA-VSA-P/SPIONs-I and AA-VSA-P/SPIONs-III at pH 9.

surface, which takes into account the chemical adsorption process of an adsorbate onto the adsorbent. This model considers that the heat of adsorption of all the molecules in the layer decreases linearly with coverage due to adsorbent−adsorbate interactions.[4,15]

The linearized form of the Langmuir isotherm model is expressed as follows:

$$\frac{1}{q_e} = \frac{1}{K_L q_m}\frac{1}{C_e} + \frac{1}{q_m} \quad (11)$$

where q_e (mg/g) represents the amount of dye adsorbed at equilibrium time for a given initial dye (adsorbate) concentration, C_e (mg/L) is the equilibrium concentration of dye in solution, q_m (mg/g) is the maximum adsorption capacity of the adsorbent, and K_L (L/mg) is the Langmuir isotherm constant.

The Freundlich adsorption isotherm model is expressed as follows:

$$q_e = K_F C_e^{1/n} \quad (12)$$

$$\log q_e = \frac{1}{n}\log C_e + \log K_F \quad (13)$$

where q_e (mg/g) and C_e (mg/g) are the amount of dye adsorbed at equilibrium time and the equilibrium dye concentration in solution, respectively, K_F (L/g) is the capacity of the adsorbent, and n is known as the heterogeneity factor. $n = 1$ implies the linear adsorption process, while $n < 1$ and $n > 1$ suggest the chemical and physical adsorption processes, respectively.[15,58]

The Temkin isotherm equation is expressed as:

$$q_e = \frac{R_0 T}{b_T}\ln(K_T C_e) \quad (14)$$

where q_e (mg/g) and C_e (mg/L) have already been defined above. R_0 and T (K) are the ideal gas constant (8.314 J/mol/K) and absolute temperature, respectively, b_T (J/mol) represents a constant related to the heat of adsorption and the positive value signifies an exothermic process, and K_T (L/g) is the equilibrium binding constant corresponding to the maximum binding energy.

To examine the type of adsorption involved in the case of the MB dye adsorption process by AA-VSA-P/SPIONs composite hydrogel systems, the study was conducted through multiple separate measurements by varying the initial dye concentration (C_0), namely, 12, 22, 33, 44, and 53 mg/L, of MB dye solutions. Representative results for the dye adsorption process of superparamagnetic composite hydrogels, AA-VSA-P/SPIONs with 1.2 and 5.2 wt % SPIONs contents (i.e., AA-VSA-P/SPIONs-I and AA-VSA-P/SPIONs-III), at pH 9 are displayed in Figure 10, where q_e (mg/g) represents the amount of dye adsorbed at equilibrium time, and C_e (mg/L) denotes the equilibrium concentration of dye in solution, as described above. Experimental data and corresponding fits with above-mentioned three best fit isotherm models, using eqs 11−13 as described above, are displayed in Figure 10. The values of the extracted parameters are presented in Table 4.

Table 4. Summary of Results for Experimental Data Fitting by Various Isotherm Models for the MB Dye Adsorption Process by Superparamagnetic Nanocomposite Hydrogels (AA-VSA-P/SPIONs) at pH 9

		AA-VSA-P/SPIONs	
isotherm model	parameter	I	III
Langmuir	K_L (L/mg)	−0.017	−0.022
	q_m (mg/g)	−33.33	−22.22
	R^2	0.98	0.88
Freundlich	K_F (L/g)	0.54	0.52
	n	0.94	0.94
	R^2	0.97	0.92
Temkin	K_T (L/g)	0.44	0.43
	b_T (J/mol)	573.5	595.5
	R^2	0.96	0.93

The negative values for the Langmuir isotherm model constants q_m and K_L, as shown in Table 4, indicate the inadequacy of the isotherm model to explain the adsorption process,[60,61] where q_m (mg/g) and K_L (L/mg) represent the maximum adsorption capacity and isotherm constant for Langmuir, respectively. Our analyses show that the Freundlich model can explain the experimental results adequately by providing a reasonably good model fit.

Normally, the value of the linear regression correlation coefficient R^2 suggests as to which model can be selected to achieve the best fit. High R^2 values for Freundlich and Temkin isotherms are evident for MB dye adsorption by AA-VSA-P/SPIONs-I and AA-VSA-P/SPIONs-III as illustrated in Table 4, indicating that the adsorption is predominantly driven by heterogeneous surfaces (adsorbent surface was heterogeneous in nature) and n values from a best fit of the Freundlich

https://doi.org/10.1021/acsomega.1c02720
ACS Omega 2021, 6, 23139−23154

isotherm model reveal the occurrence of the chemical adsorption process, which is in line with the observed high R^2 value and is well fit by the Temkin isotherm model. The result is also in agreement with the findings extracted from the study of adsorption kinetics.

2.7. Reusability/Recyclability. An excellent adsorbent should also exhibit high reusability along with its good adsorption capacity so as to minimize the overall cost of the adsorption. Additionally, in terms of practical or industrial applications, the retrieval or reuse of adsorbents is inevitable for economic growth and environmental safety.[15,27] Benefiting from the fast and efficient magnetic separation ability, the superparamagnetic nanocomposite hydrogel reported here can be easily restored. To explore the reusability of the synthesized superparamagnetic composite hydrogels AA-VSA-P/SPIONs, the studies on dye adsorption/desorption cycles were conducted. To demonstrate the reusability characteristics of the composite hydrogels, a representative MB dye adsorption/desorption study for AA-VSA-P/SPIONs-I is displayed in Figure 11. In this study, for the desorption process, acidic pH

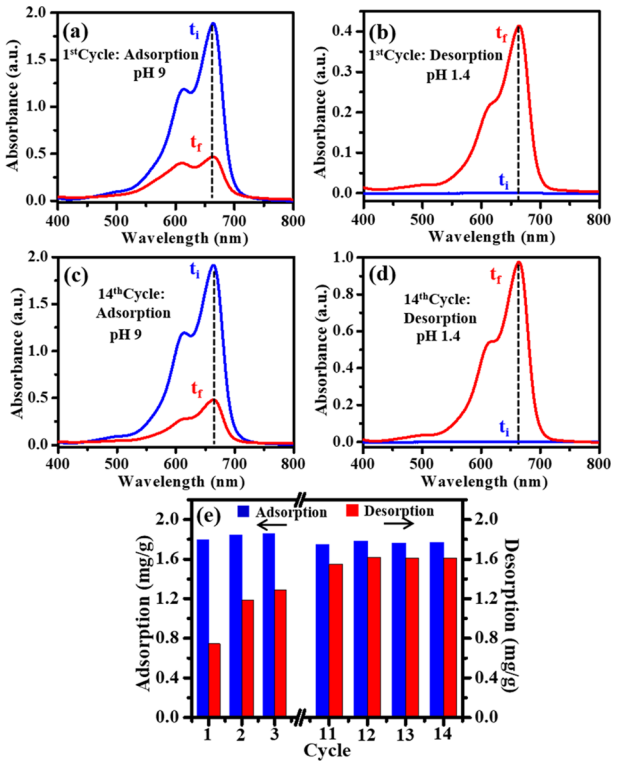

Figure 11. UV−Vis absorption spectra of MB dye solution before (t_i) and after (t_f) (a) the first cycle adsorption by AA-VSA-P/SPIONs-I at pH 9, (b) first cycle desorption by AA-VSA-P/SPIONs-I at pH 1.4, (c) 14th cycle adsorption by AA-VSA-P/SPIONs-I at pH 9, and (d) 14th cycle desorption by AA-VSA-P/SPIONs-I at pH 1.4. (e) Retention of the dye adsorption capacity of the AA-VSA-P/SPIONs-I magnetic hydrogel for 14 repeated cycles, with 12 mg/L initial dye concentration and 0.3 g of adsorbent.

medium (pH 1.4) was used based on the observed low dye adsorption capacity of the magnetic hydrogel at low pH, as discussed in Section 2.2.1.

At the first step, the dye adsorption process of AA-VSA-P/SPIONs-I was carried out for MB dye aqueous solution at alkaline pH medium (pH 9) until it saturated. In the next step, to conduct the desorption process, the dye-adsorbed AA-VSA-P/SPIONs-I magnetic hydrogel was submerged in a fresh pH 1.4 medium, and the process was repeated until the 14th cycle. The results are shown in Figure 11.

The desorption capacity was estimated through the following expression:[15]

$$q'_t = \frac{C'_t V}{W} \tag{15}$$

where q'_t (mg/g) and C'_t (mg/L) represent the desorption capacity and the instantaneous concentration of MB dye solution during the desorption process, respectively, while initially, the dye concentration C'_0 is zero, as indicated in Figure 11b,d. V (in L) and W (in g) are the volume of solution used for the desorption process and the weight of the dry magnetic hydrogel at its initial stage, respectively.

The results for dye adsorption and desorption cycles of AA-VSA-P/SPIONs-I are demonstrated in Figure 11, which specify that the synthesized AA-VSA-P/SPIONs-I preserves a decent amount of adsorption capacity even after the 14th recycling process. It has been observed that after a few cycles of recyclability, AA-VSA-P/SPIONs-I shows better stability in the adsorption−desorption process (Figure 11). Since the dye-contaminated wastewater is normally alkaline in nature based on the related industry effluent associated with dye,[8,9] and the AA-VSA-P/SPIONs magnetic hydrogel has substantial dye adsorption capacity at alkaline pH, which can also be recycled by using a low-pH solvent, the hydrogel consequently can be reused several times for the dye adsorption process. The results suggest its excellent cost effectiveness and magnetically separable platform for sustainable application of the materials in the wastewater treatment process.

2.8. Impact of the Dye Concentration on Adsorption Capacity. The impact of the initial MB dye concentration on the adsorption capacity of superparamagnetic nanocomposite hydrogels AA-VSA-P/SPIONs was explored by varying the initial MB dye concentration from 12 mg/L to 50 mg/L. Figure 12 illustrates the dye adsorption capacity of AA-VSA-P/SPIONs-I, AA-VSA-P/SPIONs-II, and AA-VSA-P/SPIONs-III for initial MB dye concentrations of 12, 30, and 50 mg/L at pH 9.

The results indicate the significant effect of the initial MB dye concentration on the dye adsorption capacity of superparamagnetic nanocomposite hydrogels AA-VSA-P/SPIONs, as displayed in Figure 12. The dye adsorption capacity of AA-VSA-P/SPIONs composite hydrogels increases with increasing initial MB dye concentration. This is due to the fact that an enhancement in the concentration of dye expedites the diffusion of the dye molecules onto the AA-VSA-P/SPIONs adsorbent as a result of an enhancement in the driving force of the concentration gradient.[50] Notably, the dye adsorption capacity of AA-VSA-P with a lower concentration of SPIONs, i.e., AA-VSA-P/SPIONs-I, is little higher than those of AA-VSA-P/SPIONs-II and AA-VSA-P/SPIONs-III, which is prominent at a higher initial dye concentration (e.g., 50 mg/L). As discussed in the earlier section (Section 2.4), the results can be ascribed to the fact that in the presence of a higher number of SPIONs, more Fe_3O_4 acted as an additional network point (through the interaction of Fe_3O_4 nanoparticles, i.e., $Fe_3O_4(OH)_x$, with COO^- and SO_3^- groups, as discussed in Section 2.2), and accordingly, the cross-link density of the hydrogel became larger, which also leads to the lowering of the available number of COO^- and SO_3^- groups to interact with

https://doi.org/10.1021/acsomega.1c02720
ACS Omega 2021, 6, 23139−23154

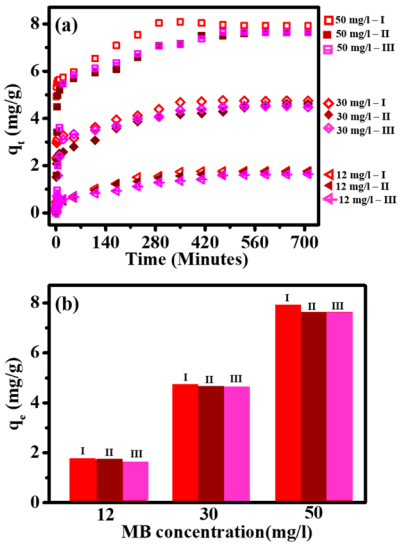

Figure 12. Effect of the initial methylene blue dye concentration on (a) the dye adsorption profile (q_t vs time) and (b) equilibrium dye adsorption capacity (q_e) of AA-VSA-P/SPIONs-I, AA-VSA-P/SPIONs-II, and AA-VSA-P/SPIONs-III (with 0.3 g of adsorbent) at pH 9 for three different MB dye concentrations: 12, 30, and 50 mg/L.

MB dye, which may cause the observed drop in the equilibrium adsorption capacity of MB dye[1,41] for the AA-VSA-P/SPIONs hydrogel with higher SPIONs content.

The MB dye adsorption capacity of AA-VSA-P/SPIONs was compared with some of the other polymeric hydrogels reported in the literature (as given in Table S1, Supporting Information). Overall, the results demonstrate the reasonably good dye adsorption performance of synthesized superparamagnetic hydrogel nanocomposites AA-VSA-P/SPIONs in terms of their dye adsorption capability even for low dye concentration, reusability, and pH sensitivity, with respect to the previously reported polymeric hydrogels for MB dye adsorption,[11,15,25,27,62,63] along with their ability to respond to the magnetic separation process in an efficient manner.

2.9. Biocompatibility Analysis. To appraise the potential of the system toward its applications in environmental remediation, or more specifically in wastewater treatment, evaluation of its biocompatibility or environment-friendliness is inevitable. The biocompatibility of the pristine hydrogel AA-VSA-P has been previously demonstrated in our earlier study.[15] Furthermore, the biocompatibility of the magnetic hydrogel nanocomposite was assessed by culturing HEK-293 cells on the synthesized AA-VSA-P/SPIONs magnetic hydrogel. Figure 13 demonstrates the confocal images of HEK-293 cells, stained with Hoechst dye, grown on AA-VSA-P/SPIONs (5 mg/mL) for 72 h. The seeded HEK-293 cells were found to adhere and proliferate on composite hydrogels AA-VSA-P/SPIONs. The excellent growth of HEK-293 cells on the magnetic hydrogel nanocomposite was observed from the fluorescence and differential interference contrast (DIC) images. The nontoxic nature and biocompatibility of the magnetic hydrogel nanocomposites can be seen by the healthy morphology of the HEK-293 cells, as indicated in the DIC images (Figure 13). The results indicate the nontoxic nature of the synthesized superparamagnetic nanocomposite hydrogels AA-VSA-P/SPIONs, implying the potential applications in wastewater treatment as an environment-friendly adsorbent.[15,64]

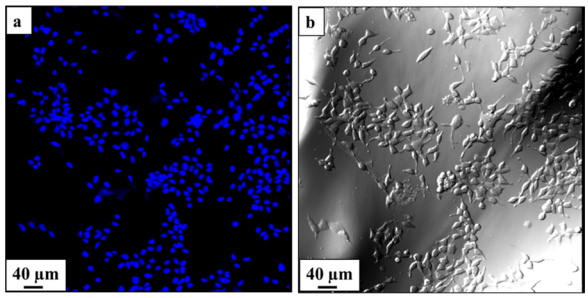

Figure 13. (a) Fluorescence and (b) differential interference contrast (DIC) images of HEK-293 cells incubated with AA-VSA-P/SPIONs (AA-VSA-P with 3.2 wt % SPIONs, i.e., AA-VSA-P/SPIONs-II) for 72 h.

3. CONCLUSIONS

In summary, the dye adsorption performance of a synthesized AA-VSA-P hydrogel after the introduction of superparamagnetic properties into it, by incorporating SPIONs (i.e., Fe_3O_4 nanoparticles), has been studied in this report. The introduction of superparamagnetic properties into the AA-VSA-P hydrogel system yields the benefits of achieving a magnetically separable system, which is important for the separation of the dye-adsorbed hydrogels for wastewater treatment. The kinetics, isotherms, and mechanism of the dye adsorption process of a synthesized superparamagnetic hydrogel nanocomposite, an AA-VSA-P/SPIONs system, have been studied elaborately in this study. It is worthwhile to mention that the thorough studies on the dye adsorption process, kinetics, and isotherms/mechanisms may provide a pathway of tuning in the design of composite hydrogels and consequent further improvement of the efficacy of such systems.

The results demonstrate the reasonably good dye adsorption performance of AA-VSA-P/SPIONs in terms of their MB dye adsorption capability even for low dye concentration, reusability or cost effectiveness, thermal stability, and high pH sensitivity, with respect to the previously reported polymeric hydrogels,[11,15,25,27,62,63] along with their ability to respond to the magnetic separation process in an efficient manner. Moreover, the observed biocompatibility of this superparamagnetic nanocomposite hydrogel indicates its potential for wastewater treatment and environmental remediation.

This study demonstrates that the synthesized AA-VSA-P/SPIONs composite hydrogels with different weight percentages of SPIONs have the combination of properties including pH sensitivity, thermal stability, substantial dye adsorption capacity, recyclability/reusability or cost effectiveness, and biocompatibility/environment-friendliness along with the superparamagnetic properties, which makes the system easily separable from the aqueous solution after the dye adsorption, by the magnetic separation process (an important requirement for the wastewater treatment). These results show that the superparamagnetic hydrogel nanocomposites AA-VSA-P/SPIONs can be utilized as a cost-effective, efficient dye adsorbent for wastewater treatment in environmental applications.

4. EXPERIMENTAL SECTION

4.1. Materials. Synthesis of dual-responsive superparamagnetic hydrogel nanocomposites, AA-VSA-P/SPIONs, with

https://doi.org/10.1021/acsomega.1c02720
ACS Omega 2021, 6, 23139−23154

different concentration of SPIONs (Fe_3O_4) was conducted using acrylic acid (AA) (Sigma-Aldrich), vinylsulfonic acid (VSA) (Sigma-Aldrich) monomers, benzoyl peroxide (BPO) (Himedia) initiator, and ethylene glycol dimethacrylate (EGDMA) (Alfa Aesar) cross-linker along with synthesized SPIONs. To synthesize SPIONs, iron(II) chloride tetrahydrate ($FeCl_2{\cdot}4H_2O$) (Sigma-Aldrich) and iron(III) chloride hexahydrate ($FeCl_3{\cdot}6H_2O$) (Sigma-Aldrich) were used. The study on dye adsorption properties of the superparamagnetic hydrogels, AA-VSA-P/SPIONs, was carried out using methylene blue (MB) dye (Sigma-Aldrich). The required aqueous solutions were prepared with deionized water, whereas the pH of aqueous solutions was maintained by adding suitable amounts of HCl (0.05 M) or NaOH (0.05 M) solutions (Merck).

4.2. Synthesis of Dual-Responsive Superparamagnetic Hydrogels, AA-VSA-P/SPIONs with Different Concentrations of SPIONs. In this work, AA-VSA-P/SPIONs with different concentrations of SPIONs were synthesized. At the initial step, a set of superparamagnetic iron oxide magnetic nanoparticles (SPIONs, Fe_3O_4) was prepared separately using a chemical coprecipitation technique as discussed in detail in our previous study.[28] Then, in the next step, sets of AA-VSA-P/SPIONs superparamagnetic hydrogel composites with different weight percentages of SPIONs, i.e., 1.2 wt % SPIONs (namely, AA-VSA-P/SPIONs-I), 3.2 wt % SPIONs (namely, AA-VSA-P/SPIONs-II), and 5.2 wt % SPIONs (namely, AA-VSA-P/SPIONs-III), were synthesized.

AA-VSA-P/SPIONs with different concentrations (wt %) of SPIONs were synthesized using the free-radical polymerization method with acrylic acid (AA) and vinylsulfonic acid (VSA) as monomers[65] in the presence of different weight percentages of presynthesized SPIONs.[66] A solution of AA and VSA with an optimized weight ratio of 5:1 (as discussed in our previous study[15]) and a weighted amount of EGDMA and BPO was prepared under constant stirring for 30 min. Then, different weight percentages of SPIONs (i.e., 1.2, 3.2, and 5.2 wt %) were added to the above-prepared solution to grow the different sets of AA-VSA-P/SPIONs samples (i.e., AA-VSA-P/SPIONs-I, AA-VSA-P/SPIONs-II, and AA-VSA-P/SPIONs-III, respectively). Milli-Q water was added to achieve the final weight up to 50 g. These mixture solutions were continuously stirred for 1 h, and the solutions were then transferred into the glass tube and purged with nitrogen gas for 2 h to eliminate the air bubbles. Further, to complete the gelation process, the prepared solutions were placed in a water bath for 48 h at 50 °C to get the different sets of AA-VSA-P/SPIONs samples (e.g., AA-VSA-P/SPIONs-I, AA-VSA-P/SPIONs-II, and AA-VSA-P/SPIONs-III). After cooling down the solutions to room temperature, the different sets of AA-VSA-P/SPIONs samples were obtained, which were further washed with an ethanol−water solution (50:50 v/v) to eliminate the unreacted monomers. The obtained superparamagnetic hydrogels were oven-dried at 60 °C until a constant weight was attained. The schematic of the formation of AA-VSA-P/SPIONs hydrogels with different concentrations (wt %) of SPIONs is shown in Figure 1a,b.

4.3. Characterization Techniques. X-ray diffraction (XRD) with CuKα radiation (λ = 1.54 Å) using a Rigaku SmartLab automated multipurpose X-ray diffractometer was used to investigate the structural properties and crystallinity of the SPIONs (i.e., Fe_3O_4 nanoparticles) and different sets of AA-VSA-P/SPIONs samples containing different wt % of SPIONs, i.e., AA-VSA-P/SPIONs-I, AA-VSA-P/SPIONs-II, and AA-VSA-P/SPIONs-III.

ATR-FTIR spectra of SPIONs, AA-VSA-P hydrogel, AA-VSA-P/SPIONs-I, AA-VSA-P/SPIONs-II, and AA-VSA-P/SPIONs-III superparamagnetic hydrogels were recorded in the range of 4000−400 cm^{-1} with a Fourier transform infrared spectrometer (PerkinElmer Spectrum Two).

The Raman scattering study was conducted in the range of 1900−150 cm^{-1} for the samples using a Raman spectrophotometer (LabRAM HR Evolution, Horiba Scientific) with a 633 nm He−Ne laser of 0.1 mW power focused onto a spot size of 0.8 mm in diameter.

Thermogravimetric analysis was accomplished to determine the thermal stability of the AA-VSA-P/SPIONs systems for different weight percentages of SPIONs using a Mettler Toledo thermal analysis system. Samples (∼7.6 mg) were heated from room temperature to 800 °C at a heating rate of 10 °C/min in a nitrogen atmosphere.

The magnetic properties (magnetization, M) of SPIONs (i.e., Fe_3O_4 nanoparticles) and the AA-VSA-P/SPIONs systems with 1.2 and 3.2 wt % SPIONs (i.e., AA-VSA-P/SPIONs-I and AA-VSA-P/SPIONs-II, respectively) were measured at room temperature (25 °C) in a magnetic field varying from −3 to +3 T using a Quantum Design MPMS XL superconducting quantum interference device magnetometer (MPMS XL, Evercool model).

A UV−Vis spectrophotometer (PerkinElmer Lambda-35) was utilized for the spectrophotometric measurements with a spectral range of 200−800 nm to study the dye adsorption properties of the different sets of AA-VSA-P/SPIONs samples (i.e., AA-VSA-P/SPIONs-I, AA-VSA-P/SPIONs-II, and AA-VSA-P/SPIONs-III). For the biocompatibility evaluation of the AA-VSA-P/SPIONs hydrogel, the cells' viability was determined by imaging live cells using confocal microscopy (Olympus confocal laser scanning microscope).

4.4. Dye Adsorption Experiments. The dye adsorption measurements were conducted for the AA-VSA-P/SPIONs composite hydrogels having different weight percentages (1.2, 3.2, and 5.2 wt %) of SPIONs (i.e., AA-VSA-P/SPIONs-I, AA-VSA-P/SPIONs-II, and AA-VSA-P/SPIONs-III) using methylene blue (MB) dye to study their capability to remove cationic dye. Three sets of systems were prepared by adding approximately 0.3 g of AA-VSA-P/SPIONs-I, AA-VSA-P/SPIONs-II, and AA-VSA-P/SPIONs-III composite hydrogels separately in three sets of 0.05 L of MB dye solutions (12 mg/L). The dye adsorption capacity was evaluated through the estimation of MB dye concentrations in the aqueous solution at different time intervals during the adsorption process, using UV−Vis absorption spectroscopy, using normalized absorbance (A/A_0) at the wavelength of 664 nm, the main peak position of the absorption spectrum, of the MB dye solution, where A_0 and A signify the initial absorbance and instantaneous absorbance, respectively.

4.5. Reusability/Recyclability Experiments. The adsorption and desorption cycles were performed to test the reusability/recyclability performance of the synthesized AA-VSA-P/SPIONs for dye adsorption application. At first, 0.3 g of AA-VSA-P/SPIONs (AA-VSA-P/SPIONs-I) hydrogel was immersed in 0.05 L of MB dye aqueous solution (12 mg/L) at high/alkaline pH (pH 9). The superparamagnetic hydrogel's dye adsorption capacity was conducted for the first cycle. After completing the adsorption process for the first cycle, the superparamagnetic hydrogel samples loaded with MB dye were

https://doi.org/10.1021/acsomega.1c02720
ACS Omega 2021, 6, 23139−23154

separated out and then added to 0.05 L of another fresh low pH (pH 1.4) aqueous solution. After the desired time interval, the AA-VSA-P/SPIONs hydrogel was separated out from the solution. The amount of dye desorbed was estimated using a UV−Vis absorption spectrophotometer by the measured MB dye concentration in low pH aqueous solution. After the first desorption, the AA-VSA-P/SPIONs hydrogel was next reused for the second adsorption cycle. Following the above-mentioned process, the reusability study was performed for 14 consecutive cycles.

4.6. Biocompatibility Evaluation of the AA-VSA-P/SPIONs Hydrogel. The viability assay of human embryonic kidney cells (HEK-293) on the AA-VSA-P/SPIONs hydrogel was conducted to determine its biocompatibility. The sterilization of the dried AA-VSA-P/SPIONs at an increasing concentration (0.1, 1, 2, 3, 4, 5, and 10 mg/mL) was first performed using 70% ethanol and then irradiated under UV light. The equilibration of the superparamagnetic hydrogel was conducted for 1 h using sterile phosphate buffer solution (PBS) (1.5 mL/well) in a 12-well plate. PBS was first aspirated from the plate and hydrogels were kept in DMEM medium (1.5 mL/well) supplemented with 10% FBS, 1% sodium pyruvate, and 1% penicillin/streptomycin solution and incubated overnight at 37 °C. After removing the spent medium from the plate, the HEK-293 cells (10,000 cells/well, 1.5 mL medium) were seeded on the superparamagnetic hydrogels. The cells were incubated for 72 h in the magnetic hydrogel and were then stained with Hoechst 33342 dye (5 μM, 1.5 mL/well) for 25 min, followed by PBS wash (3 × 2 mL). The cells' viability was determined through an imaging technique using confocal microscopy (Olympus confocal laser scanning microscope) with an excitation at 405 nm.

■ ASSOCIATED CONTENT

Supporting Information

The Supporting Information is available free of charge at https://pubs.acs.org/doi/10.1021/acsomega.1c02720.

> Image showing the effect of a higher weight percentage of SPIONs (above 6 wt %), resulting in an impairment in the hydrogel formation process (Figure S1); TEM image of superparamagnetic iron oxide nanoparticles, SPIONs (Figure S2); comparison of the adsorption capacities of AA-VSA-P/SPIONs-I hydrogel and other reported polymeric hydrogels for the removal of MB dye (Table S1); plot of magnetization (M) as a function of the applied magnetic field (H) for AA-VSA-P with 1.2 wt % SPIONs and 3.2% SPIONs (Figure S3); dye adsorption properties of AA-VSA-P/SPIONs-I for another cationic dye, rhodamine B, having a different chemical structure from MB dye (S4−S6) (PDF)

■ AUTHOR INFORMATION

Corresponding Author

Sudeshna Chattopadhyay − *Department of Biosciences and Biomedical Engineering, Department of Physics, and Department of Metallurgy Engineering and Materials Science, Indian Institute of Technology Indore, Indore 453552, India;* orcid.org/0000-0002-6151-5871;
Email: chattopadhyay.sudeshna@gmail.com, sudeshna@iiti.ac.in

Authors

Rinki Singh − *Department of Biosciences and Biomedical Engineering, Indian Institute of Technology Indore, Indore 453552, India*

Vikas Munya − *Department of Physics, Indian Institute of Technology Indore, Indore 453552, India*

Venkata Narayana Are − *Department of Biosciences and Biomedical Engineering, Indian Institute of Technology Indore, Indore 453552, India*

Debasis Nayak − *Department of Biosciences and Biomedical Engineering, Indian Institute of Technology Indore, Indore 453552, India;* orcid.org/0000-0002-4762-4553

Complete contact information is available at: https://pubs.acs.org/10.1021/acsomega.1c02720

Notes

The authors declare no competing financial interest.

■ ACKNOWLEDGMENTS

We would like to acknowledge IIT Indore for all kinds of support to this work and the Sophisticated Instrument Centre (SIC), IIT Indore. We would also like to acknowledge project no. SR/FST/PSI/225/2016 under the FIST program of DST, Government of India, for the Raman characterization facility. We also acknowledge Saha Institute of Nuclear Physics, Kolkata, for providing the transmission electron microscopy (TEM) facility, the Unit of Nanoscience at Indian Association for the Cultivation of Science (IACS), Kolkata, for the support of magnetization measurements, and the DST, Government of India, for funding of the Quantum Design MPMS XL superconducting quantum interference device magnetometer (MPMS XL, Evercool model) used in this study. We would like to acknowledge the help of Dr. Debasis Nayak, IIT Indore, and his group for the cytotoxicity study. This work is partially supported by the Science and Engineering Research Board (SERB), India, project no. CRG/2020/005595. R.S. is thankful to DST-INDIA, New Delhi, under award no. IF150378 and V.M. is thankful to CSIR-UGC, New Delhi, under UGC-ref. no. 1364/(CSIR-UGC NET JUNE 2018) for providing the fellowships.

■ REFERENCES

(1) Xie, Z.-W.; Lin, J.-C.; Xu, M.-Y.; Wang, H.-Y.; Wu, Y.-X.; He, F.-A.; Jiang, H.-L. Novel Fe_3O_4 Nanoparticle/β-Cyclodextrin-Based Polymer Composites for the Removal of Methylene Blue from Water. *Ind. Eng. Chem. Res.* **2020**, *59*, 12270−12281.

(2) Katheresan, V.; Kansedo, J.; Lau, S. Y. Efficiency of various recent wastewater dye removal methods: a review. *J. Environ. Chem. Eng.* **2018**, *6*, 4676−4697.

(3) Ginimuge, P. R.; Jyothi, S. Methylene blue: revisited. *J. Anaesthesiol., Clin. Pharmacol.* **2010**, *26*, 517.

(4) Mittal, H.; Babu, R.; Dabbawala, A. A.; Alhassan, S. M. Low-Temperature Synthesis of Magnetic Carbonaceous Materials Coated with Nanosilica for Rapid Adsorption of Methylene Blue. *ACS Omega* **2020**, *5*, 6100−6112.

(5) Yagub, M. T.; Sen, T. K.; Ang, H. Equilibrium, kinetics, and thermodynamics of methylene blue adsorption by pine tree leaves. *Water, Air, Soil Pollut.* **2012**, *223*, 5267−5282.

(6) Du, J.; Yang, X.; Xiong, H.; Dong, Z.; Wang, Z.; Chen, Z.; Zhao, L. Ultrahigh Adsorption Capacity of Acrylic Acid-Grafted Xanthan Gum Hydrogels for Rhodamine B from Aqueous Solution. *J. Chem. Eng. Data* **2021**, *66*, 1264−1272.

(7) Choe, E. K.; Son, E. J.; Lee, B. S.; Jeong, S. H.; Shin, H. C.; Choi, J. S. NF process for the recovery of caustic soda and concentration of

disodium terephthalate from alkaline wastewater from polyester fabrics. *Desalination* **2005**, *186*, 29−37.
(8) Shen, C.; Shen, Y.; Wen, Y.; Wang, H.; Liu, W. Fast and highly efficient removal of dyes under alkaline conditions using magnetic chitosan-Fe (III) hydrogel. *Water Res.* **2011**, *45*, 5200−5210.
(9) Wang, Z.; Xue, M.; Huang, K.; Liu, Z. Textile dyeing wastewater treatment. *Adv. Treat. Text Effluent.* **2011**, *5*, 91−116.
(10) Rotte, N. K.; Yerramala, S.; Boniface, J.; Srikanth, V. V. S. S. Equilibrium and kinetics of Safranin O dye adsorption on MgO decked multi-layered graphene. *Chem. Eng. J.* **2014**, *258*, 412−419.
(11) Song, W.; Gao, B.; Xu, X.; Xing, L.; Han, S.; Duan, P.; Song, W.; Jia, R. Adsorption−desorption behavior of magnetic amine/Fe_3O_4 functionalized biopolymer resin towards anionic dyes from wastewater. *Bioresour. Technol.* **2016**, *210*, 123−130.
(12) Zhang, J.; Azam, M. S.; Shi, C.; Huang, J.; Yan, B.; Liu, Q.; Zeng, H. Poly (acrylic acid) functionalized magnetic graphene oxide nanocomposite for removal of methylene blue. *RSC Adv.* **2015**, *5*, 32272−32282.
(13) Zhu, S.; Jiao, S.; Liu, Z.; Pang, G.; Feng, S. High adsorption capacity for dye removal by CuZn hydroxyl double salts. *Environ. Sci. Nano* **2014**, *1*, 172−180.
(14) Rashid, T. U.; Kabir, S. F.; Biswas, M. C.; Bhuiyan, M. R. Sustainable wastewater treatment via dye−surfactant interaction: a critical review. *Ind. Eng. Chem. Res.* **2020**, *59*, 9719−9745.
(15) Singh, R.; Pal, D.; Mathur, A.; Singh, A.; Krishnan, M. A.; Chattopadhyay, S. An efficient pH sensitive hydrogel, with biocompatibility and high reusability for removal of methylene blue dye from aqueous solution. *React. Funct. Polym.* **2019**, *144*, 104346.
(16) Pal, S.; Ghorai, S.; Das, C.; Samrat, S.; Ghosh, A.; Panda, A. B. Carboxymethyl tamarind-g-poly (acrylamide)/silica: a high performance hybrid nanocomposite for adsorption of methylene blue dye. *Ind. Eng. Chem. Res.* **2012**, *51*, 15546−15556.
(17) Mezohegyi, G.; van der Zee, F. P.; Font, J.; Fortuny, A.; Fabregat, A. Towards advanced aqueous dye removal processes: a short review on the versatile role of activated carbon. *J. Environ. Manage.* **2012**, *102*, 148−164.
(18) Gautam, D.; Hooda, S. Magnetic Graphene Oxide/Chitin Nanocomposites for Efficient Adsorption of Methylene Blue and Crystal Violet from Aqueous Solutions. *J. Chem. Eng. Data* **2020**, *65*, 4052−4062.
(19) Ngah, W. W.; Teong, L.; Hanafiah, M. M. Adsorption of dyes and heavy metal ions by chitosan composites: A review. *Carbohydr. Polym.* **2011**, *83*, 1446−1456.
(20) Crini, G. Recent developments in polysaccharide-based materials used as adsorbents in wastewater treatment. *Prog. Polym. Sci.* **2005**, *30*, 38−70.
(21) Halouane, F.; Oz, Y.; Meziane, D.; Barras, A.; Juraszek, J.; Singh, S. K.; Kurungot, S.; Shaw, P. K.; Sanyal, R.; Boukherroub, R.; Sanyal, A.; Szunerits, S. Magnetic reduced graphene oxide loaded hydrogels: highly versatile and efficient adsorbents for dyes and selective Cr (VI) ions removal. *J. Colloid Interface Sci.* **2017**, *507*, 360−369.
(22) Mahdavinia, G. R.; Aghaie, H.; Sheykhloie, H.; Vardini, M. T.; Etemadi, H. Synthesis of CarAlg/MMt nanocomposite hydrogels and adsorption of cationic crystal violet. *Carbohydr. Polym.* **2013**, *98*, 358−365.
(23) Shalla, A. H.; Bhat, M. A.; Yaseen, Z. Hydrogels for removal of recalcitrant organic dyes: A conceptual overview. *J. Environ. Chem. Eng.* **2018**, *6*, 5938−5949.
(24) Yuan, Z.; Wang, Y.; Han, X.; Chen, D. The adsorption behaviors of the multiple stimulus-responsive poly (ethylene glycol)-based hydrogels for removal of RhB dye. *J. Appl. Polym. Sci.* **2015**, *132*, 42244.
(25) Sun, X.-F.; Liu, B.; Jing, Z.; Wang, H. Preparation and adsorption property of xylan/poly (acrylic acid) magnetic nanocomposite hydrogel adsorbent. *Carbohydr. Polym.* **2015**, *118*, 16−23.
(26) Cao, C.; Xiao, L.; Chen, C.; Shi, X.; Cao, Q.; Gao, L. In situ preparation of magnetic Fe3O4/chitosan nanoparticles via a novel reduction−precipitation method and their application in adsorption of reactive azo dye. *Powder Technol.* **2014**, *260*, 90−97.
(27) Gong, G.; Zhang, F.; Cheng, Z.; Zhou, L. Facile fabrication of magnetic carboxymethyl starch/poly (vinyl alcohol) composite gel for methylene blue removal. *Int. J. Biol. Macromol.* **2015**, *81*, 205−211.
(28) Singh, R.; Pal, D.; Chattopadhyay, S. Target-Specific Superparamagnetic Hydrogel with Excellent pH Sensitivity and Reversibility: A Promising Platform for Biomedical Applications. *ACS Omega* **2020**, *5*, 21768−21780.
(29) Tipsawat, P.; Wongpratat, U.; Phumying, S.; Chanlek, N.; Chokprasombat, K.; Maensiri, S. Magnetite (Fe3O4) nanoparticles: Synthesis, characterization and electrochemical properties. *Appl. Surf. Sci.* **2018**, *446*, 287−292.
(30) Hasanpour, A.; Niyaifar, M.; Asan, M.; Amighian, J. Synthesis and characterization of Fe_3O_4 and ZnO nanocomposites by the sol−gelmethod. *J. Magn. Magn. Mater.* **2013**, *334*, 41−44.
(31) Reddy, N. N.; Ravindra, S.; Reddy, N. M.; Rajinikanth, V.; Raju, K. M.; Vallabhapurapu, V. S. Temperature responsive hydrogel magnetic nanocomposites for hyperthermia and metal extraction applications. *J. Magn. Magn. Mater.* **2015**, *394*, 237−244.
(32) Zheng, Y.; Huang, D.; Wang, A. Chitosan-g-poly (acrylic acid) hydrogel with crosslinked polymeric networks for Ni^{2+} recovery. *Anal. Chim. Acta* **2011**, *687*, 193−200.
(33) Stuart, B. Spectral analysis. *Infrared Spectrosc. Fundam. Appl.* **2004**, 45−70.
(34) Dey, C.; Das, A.; Goswami, M. M. Dopamine Loaded SiO_2 Coated Fe_3O_4 Magnetic Nanoparticles: A New Anticancer Agent in pH-Dependent Drug Delivery. *ChemistrySelect* **2019**, *4*, 12190−12196.
(35) Yong, C.; Chen, X.; Xiang, Q.; Li, Q.; Xing, X. Recyclable magnetite-silver heterodimer nanocomposites with durable antibacterial performance. *Bioact. Mater.* **2018**, *3*, 80−86.
(36) Karaoğlu, E.; Baykal, A.; Şenel, M.; Sözeri, H.; Toprak, M. S. Synthesis and characterization of piperidine-4-carboxylic acid functionalized Fe3O4 nanoparticles as a magnetic catalyst for Knoevenagel reaction. *Mater. Res. Bull.* **2012**, *47*, 2480−2486.
(37) Song, Y.; Wang, R.; Rong, R.; Ding, J.; Liu, J.; Li, R.; Liu, Z.; Li, H.; Wang, X.; Zhang, J.; Fang, J. Synthesis of well-dispersed aqueous-phase magnetite nanoparticles and their metabolism as an MRI contrast agent for the reticuloendothelial system. *Eur. J. Inorg. Chem.* **2011**, *2011*, 3303−3313.
(38) Akl, Z. F.; El-Saeed, S. M.; Atta, A. M. In-situ synthesis of magnetite acrylamide amino-amidoxime nanocomposite adsorbent for highly efficient sorption of U (VI) ions. *J. Ind. Eng. Chem.* **2016**, *34*, 105−116.
(39) Faghihi, K.; Raeisi, A.; Amini, M.; Shabanian, M.; Karimi, A. R. Sulfonic acid-functionalized Fe_3O_4 reinforced soluble polyimide: synthesis and properties. *Polym.-Plast. Technol. Eng.* **2016**, *55*, 259−267.
(40) Mittal, H.; Maity, A.; Ray, S. S. Effective removal of cationic dyes from aqueous solution using gum ghatti-based biodegradable hydrogel. *Int. J. Biol. Macromol.* **2015**, *79*, 8−20.
(41) Pooresmaeil, M.; Mansoori, Y.; Mirzaeinejad, M.; Khodayari, A. Efficient removal of methylene blue by novel magnetic hydrogel nanocomposites of poly (acrylic acid). *Adv. Polym. Technol.* **2018**, *37*, 262−274.
(42) Zhou, C.; Wu, Q.; Lei, T.; Negulescu, I. I. Adsorption kinetic and equilibrium studies for methylene blue dye by partially hydrolyzed polyacrylamide/cellulose nanocrystal nanocomposite hydrogels. *Chem. Eng. J.* **2014**, *251*, 17−24.
(43) Sharma, G.; Kumar, A.; Devi, K.; Sharma, S.; Naushad, M.; Ghfar, A. A.; Ahamad, T.; Stadler, F. J. Guar gum-crosslinked-Soya lecithin nanohydrogel sheets as effective adsorbent for the removal of thiophanate methyl fungicide. *Int. J. Biol. Macromol.* **2018**, *114*, 295−305.
(44) Kemik, Ö. F.; Ngwabebhoh, F. A.; Yildiz, U. A response surface modelling study for sorption of Cu^{2+}, Ni2+, Zn^{2+} and Cd^{2+} using chemically modified poly (vinylpyrrolidone) and poly (vinyl-

https://doi.org/10.1021/acsomega.1c02720
ACS Omega 2021, 6, 23139−23154

pyrrolidone-co-methylacrylate) hydrogels. *Adsorp. Sci. Technol.* **2017**, *35*, 263−283.
(45) Tan, K. L.; Hameed, B. H. Insight into the adsorption kinetics models for the removal of contaminants from aqueous solutions. *J. Taiwan Inst. Chem. Eng.* **2017**, *74*, 25−48.
(46) Pour, Z. S.; Ghaemy, M. Removal of dyes and heavy metal ions from water by magnetic hydrogel beads based on poly (vinyl alcohol)/carboxymethyl starch-g-poly (vinyl imidazole). *RSC Adv.* **2015**, *5*, 64106−64118.
(47) Ho, Y. S.; McKay, G. A comparison of chemisorption kinetic models applied to pollutant removal on various sorbents. *Process Saf. Environ. Prot.* **1998**, *76*, 332−340.
(48) Jana, S.; Ray, J.; Bhanja, S. K.; Tripathy, T. Removal of textile dyes from single and ternary solutions using poly (acrylamide-co-N-methylacrylamide) grafted katira gum hydrogel. *J. Appl. Polym. Sci.* **2018**, *135*, 44849.
(49) Pérez-Marín, A.; Zapata, V. M.; Ortuno, J.; Aguilar, M.; Sáez, J.; Lloréns, M. Removal of cadmium from aqueous solutions by adsorption onto orange waste. *J. Hazard. Mater.* **2007**, *139*, 122−131.
(50) Jv, X.; Zhao, X.; Ge, H.; Sun, J.; Li, H.; Wang, Q.; Lu, H. Fabrication of a magnetic poly (aspartic acid)-poly (acrylic acid) hydrogel: application for the adsorptive removal of organic dyes from aqueous solution. *J. Chem. Eng. Data* **2019**, *64*, 1228−1236.
(51) Wu, F.-C.; Tseng, R.-L.; Juang, R.-S. Characteristics of Elovich equation used for the analysis of adsorption kinetics in dye-chitosan systems. *Chem. Eng. J.* **2009**, *150*, 366−373.
(52) Chang, Z.; Chen, Y.; Tang, S.; Yang, J.; Chen, Y.; Chen, S.; Li, P.; Yang, Z. Construction of chitosan/polyacrylate/graphene oxide composite physical hydrogel by semi-dissolution/acidification/sol-gel transition method and its simultaneous cationic and anionic dye adsorption properties. *Carbohydr. Polym.* **2020**, *229*, 115431.
(53) Shi, H.; Li, W.; Zhong, L.; Xu, C. Methylene blue adsorption from aqueous solution by magnetic cellulose/graphene oxide composite: equilibrium, kinetics, and thermodynamics. *Ind. Eng. Chem. Res.* **2014**, *53*, 1108−1118.
(54) Jing, Z.; Zhang, G.; Sun, X. F.; Shi, X.; Sun, W. Preparation and adsorption properties of a novel superabsorbent based on multiwalled carbon nanotubes−xylan composite and poly (methacrylic acid) for methylene blue from aqueous solution. *Polym. Compos.* **2014**, *35*, 1516−1528.
(55) Dragan, E. S.; Perju, M. M.; Dinu, M. V. Preparation and characterization of IPN composite hydrogels based on polyacrylamide and chitosan and their interaction with ionic dyes. *Carbohydr. Polym.* **2012**, *88*, 270−281.
(56) Mahdavinia, G. R.; Massoudi, A.; Baghban, A.; Shokri, E. Study of adsorption of cationic dye on magnetic kappa-carrageenan/PVA nanocomposite hydrogels. *J. Environ. Chem. Eng.* **2014**, *2*, 1578−1587.
(57) Singh, N.; Riyajuddin, S.; Ghosh, K.; Mehta, S. K.; Dan, A. Chitosan-Graphene Oxide Hydrogels with Embedded Magnetic Iron Oxide Nanoparticles for Dye Removal. *ACS Appl. Nano Mater.* **2019**, *2*, 7379−7392.
(58) Vargas, A. M. M.; Cazetta, A. L.; Kunita, M. H.; Silva, T. L.; Almeida, V. C. Adsorption of methylene blue on activated carbon produced from flamboyant pods (Delonix regia): Study of adsorption isotherms and kinetic models. *Chem. Eng. J.* **2011**, *168*, 722−730.
(59) Gimbert, F.; Morin-Crini, N.; Renault, F.; Badot, P.-M.; Crini, G. Adsorption isotherm models for dye removal by cationized starch-based material in a single component system: error analysis. *J. Hazard. Mater.* **2008**, *157*, 34−46.
(60) Kayranli, B. Adsorption of textile dyes onto iron based waterworks sludge from aqueous solution; isotherm, kinetic and thermodynamic study. *Chem. Eng. J.* **2011**, *173*, 782−791.
(61) Ramakrishna, K. R.; Viraraghavan, T. Dye removal using low cost adsorbents. *Water Sci. Technol.* **1997**, *36*, 189−196.
(62) Mahmoud, M. E.; Abdelwahab, M. S. Fabricated and functionalized magnetite/phenylenediamine/cellulose acetate nano-composite for adsorptive removal of methylene blue. *Int. J. Biol. Macromol.* **2019**, *128*, 196−203.
(63) Sanchez, L. M.; Actis, D. G.; Gonzalez, J. S.; Zélis, P. M.; Alvarez, V. A. Effect of PAA-coated magnetic nanoparticles on the performance of PVA-based hydrogels developed to be used as environmental remediation devices. *J. Nanopart. Res.* **2019**, *21*, 1−16.
(64) Wiemer, K.; Dörmbach, K.; Slabu, I.; Agrawal, G.; Schrader, F.; Caumanns, T.; Bourone, S.; Mayer, J.; Steitz, J.; Simon, U.; Pich, A. Hydrophobic superparamagnetic FePt nanoparticles in hydrophilic poly (N-vinylcaprolactam) microgels: a new multifunctional hybrid system. *J. Mater. Chem. B* **2017**, *5*, 1284−1292.
(65) Huang, Y.; Liu, M.; Chen, J.; Gao, C.; Gong, Q. A novel magnetic triple-responsive composite semi-IPN hydrogels for targeted and controlled drug delivery. *Eur. Polym. J.* **2012**, *48*, 1734−1744.
(66) Zhou, L.; He, B.; Zhang, F. Facile one-pot synthesis of iron oxide nanoparticles cross-linked magnetic poly (vinyl alcohol) gel beads for drug delivery. *ACS Appl. Mater. Interfaces* **2012**, *4*, 192−199.

https://doi.org/10.1021/acsomega.1c02720
ACS Omega 2021, 6, 23139−23154